A&A 564, A39 (2014)
DOI: 10.1051/0004-6361/201322798

Astronomy & Astrophysics

The VLT-FLAMES Tarantula Survey⋆,⋆⋆

XIII: On the nature of O Vz stars in 30 Doradus

C. Sabín-Sanjulián[1,2], S. Simón-Díaz[1,2], A. Herrero[1,2], N. R. Walborn[3], J. Puls[4], J. Maíz Apellániz[5], C. J. Evans[6], I. Brott[7], A. de Koter[8,9], M. Garcia[10], N. Markova[11], F. Najarro[10], O. H. Ramírez-Agudelo[8], H. Sana[3], W. D. Taylor[6], and J. S. Vink[12]

[1] Instituto de Astrofísica de Canarias, 38200 La Laguna, Tenerife, Spain
e-mail: cssj@iac.es
[2] Departamento de Astrofísica, Universidad de La Laguna, 38205 La Laguna, Tenerife, Spain
[3] Space Telescope Science Institute, 3700 San Martin Drive, Baltimore MD 21218, USA
[4] Universitäts-Sternwarte, Scheinerstrasse 1, 81679 München, Germany
[5] Instituto de Astrofísica de Andalucía-CSIC, Glorieta de la Astronomía s/n, 18008 Granada, Spain
[6] UK Astronomy Technology Centre, Royal Observatory Edinburgh, Blackford Hill, Edinburgh EH9 3HJ, UK
[7] University of Vienna, Department of Astrophysics, Türkenschanzstr. 17, 1180 Vienna, Austria
[8] Astronomical Institute Anton Pannekoek, University of Amsterdam, Kruislaan 403, 1098 SJ Amsterdam, The Netherlands
[9] Instituut voor Sterrenkunde, Universiteit Leuven, Celestijnenlaan 200 D, 3001 Leuven, Belgium
[10] Centro de Astrobiología (CSIC-INTA), Ctra. de Torrejón a Ajalvir km-4, 28850 Torrejón de Ardoz, Madrid, Spain
[11] Institute of Astronomy with NAO, Bulgarian Academy of Sciences, PO Box 136, 4700 Smoljan, Bulgaria
[12] Armagh Observatory, College Hill, Armagh BT61 9DG, UK

Received 4 October 2013 / Accepted 4 December 2013

ABSTRACT

Context. O Vz stars, a subclass of O-type dwarfs characterized by having He II λ4686 stronger in absorption than any other helium line in their blue-violet spectra, have been suggested to be on or near the zero-age main sequence (ZAMS). If their youth were confirmed, they would be key objects with which to advance our knowledge of the physical properties of massive stars in the early stages of their lives.
Aims. We test the hypothesis of O Vz stars being at a different (younger) evolutionary stage than are normal O-type dwarfs.
Methods. We have performed the first comprehensive quantitative spectroscopic analysis of a statistically meaningful sample of O Vz and O V stars in the same star-forming region, exploiting the large number of O Vz stars identified by the VLT-FLAMES Tarantula Survey in the 30 Doradus region of the Large Magellanic Cloud (LMC). We obtained the stellar and wind parameters of 38 O Vz stars (and a control sample of 46 O V stars) using the FASTWIND stellar atmosphere code and the IACOB-GBAT, a grid-based tool developed for automated quantitative analysis of optical spectra of O stars. In the framework of a differential study, we compared the physical and evolutionary properties of both samples, locating the stars in the $\log g$ vs. $\log T_{\rm eff}$, $\log Q$ vs. $\log T_{\rm eff}$, and $\log L/L_{\odot}$ vs. $\log T_{\rm eff}$ diagrams. We also investigated the predictions of the FASTWIND code regarding the O Vz phenomenon.
Results. We find a differential distribution of objects in terms of effective temperature, with O Vz stars dominant at intermediate values. The O Vz stars in 30 Doradus tend to be younger (i.e., closer to the ZAMS) and less luminous, and they have weaker winds than the O V stars, but we also find examples with ages of 2−4 Myr and with luminosities and winds that are similar to those of normal O dwarfs. Moreover, the O Vz stars do not appear to have higher gravities than the O V stars. In addition to effective temperature and wind strength, our FASTWIND predictions indicate how important it is to take other stellar parameters (gravity and projected rotational velocity) into account for correctly interpreting the O Vz phenomenon.
Conclusions. In general, the O Vz stars appear to be on or very close to the ZAMS, but there are some examples where the Vz classification does not necessarily imply extreme youth. In particular, the presence of O Vz stars in our sample at more evolved phases than expected is likely a consequence of modest O-star winds owing to the low-metallicity environment of the LMC.

Key words. Magellanic Clouds – stars: atmospheres – stars: early-type – stars: fundamental parameters – stars: massive

1. Introduction

One of the open questions in the formation and evolution of massive stars is what is the first stage of their lives. A typical high-mass protostar is formed in a molecular cloud, accumulating mass with an accretion timescale that could be longer than the contraction timescale (see Bernasconi & Maeder 1996). This would lead to a situation in which a high-mass star begins to burn hydrogen in its core while still accreting material from the parental cloud. This zero-age main sequence (ZAMS) star would appear embedded and optically obscured in the molecular cloud, even if it is already emitting ultraviolet photons and has created a small Strömgren sphere around it (Churchwell 2002). Massive stars may spend ∼15% of their lifetime in this embedded stage (Zinnecker & Yorke 2007, and references therein). When the parental cloud is sufficiently dissolved, it is easier to observe the

⋆ Based on observations at the European Southern Observatory Very Large Telescope in program 182.D-0222.
⋆⋆ Appendices are available in electronic form at http://www.aanda.org

star at optical wavelengths, but it is already somewhat evolved. The ZAMS stage of massive stars is therefore very difficult to observe at wavelengths where the main diagnostics of stellar parameters are concentrated, i.e., the ultraviolet, optical, and although to a lesser extent, the near-infrared (see Hanson 1998).

To learn more about the final stage of formation of massive stars, it is interesting to identify objects that have just passed their birthline, since these may reveal remnant signatures of the formation process. Over recent decades, observations of O-type dwarfs in the Milky Way (MW) and the Magellanic Clouds have opened up optical studies of O stars apparently on or close to the ZAMS. Walborn (1973) commented on the presence of O dwarfs in the Tr14 cluster (Carina nebula), which displayed higher He II λ4686/He II λ4541 absorption-line ratios than in normal dwarfs. This spectroscopic feature motivated the definition of a new luminosity subclass, Vz, in which He II λ4686 is deeper than both He I λ4471 and He II λ4541.

The O Vz phenomenon has been suggested to be an "inverse" Of effect. In Of stars, He II λ4686 goes from absorption to emission when moving from the mildest O((f)) cases to the most extreme Of examples. This effect is due to the intensity of the stellar wind, which increases with luminosity and when the star evolves and departs from main sequence. Following this reasoning, the strong He II λ4686 absorption in O Vz stars could be explained by less wind emission filling the line in than in typical O V stars. In this scenario, O Vz stars are said to be objects on (or near) the ZAMS, with lower luminosities and weaker winds than normal O dwarfs (Walborn 2009). Therefore, O Vz stars would represent the link between the early phases of star formation (such as ultra-compact H II regions) and the normal, already slightly evolved, O dwarfs. Moreover, being young and subluminous, they could also offer a link to the so-called "weak-wind" stars, which are found to have weaker winds than predicted by the theory of radiatively driven winds (Bouret et al. 2003; Martins et al. 2005). The reasons for these weak winds are currently under debate but it is thought that, below a certain luminosity threshold, stars are not able to initiate their outflows by radiation pressure alone (see Lucy 2010; Muijres et al. 2012).

Many stars have been classified as O Vz after introduction of the subclass (viz. Morrell et al. 1991; Parker et al. 1992; Walborn & Parker 1992; Walborn & Blades 1997; Parker et al. 2001). Others have been proposed as belonging to it owing to the presence of characteristics that may be linked to the Vz subclass (like the subluminosity or the weak winds, see e.g., Heydari-Malayeri et al. 2002). We also refer the reader to the review by Walborn (2009), who presented a compilation of the 25 O Vz stars known at the time[1], located in the Galaxy and Magellanic Clouds.

Despite the potential relevance of O Vz stars to the formation and early evolution of massive stars, only a few have been quantitatively analyzed to date. Intringuingly, the limited number of quantitative results place some on the ZAMS, such as HD 93 128 (Repolust et al. 2004) and HD 152 590 (Martins et al. 2005), while others are seen to depart from the ZAMS, e.g., HD 42 088 (Martins et al. 2005) and more recently CPD-582 620 and HD 91 824 (Markova et al. 2014).

Three O Vz stars in the Small Magellanic Cloud (SMC) were analyzed by Mokiem et al. (2006), who found that two (NGC 346-028 and NGC 346-051) lay close to the ZAMS (but, curiously, with enriched helium abundances, which point to a more evolved stage), while the third (NGC 346-031) appeared older. These stars have recently been analyzed by Bouret et al. (2013) who, in agreement with Mokiem et al., estimated NGC 346-031 to be older than 2.5 Myr (but with a lower helium abundance and mass-loss rate) and placed NGC 346-051 close to the ZAMS (younger than 1 Myr). However, in contrast to Mokiem et al., they found NGC 346-028 to be separated from the ZAMS (at 2−3 Myr). Interestingly, they reported an enhanced N/O abundance for NGC 346-051 and indicate that, despite its apparent proximity to the ZAMS, this star could actually be a more evolved, fast rotator.

A similar puzzling situation was found by Martins et al. (2012). Their analysis of HD 46 150 and HD 46 573 found that these two O Vz stars are nitrogen enriched and not particularly closer to the ZAMS than other O V stars. However, HD 46 573 is a known binary (Mason et al. 1998) and HD 46 150 is a candidate binary (Mahy et al. 2009), which could affect both the spectral classification and interpretation of the quantitative results. The recent case of HD 150 136 is also interesting as Mahy et al. (2012) found that it is part of a triple system, where the primary presents an incipient P-Cygni profile for He II λ4686. After spectral disentangling, the other two components display O Vz characteristics (although the case of the third component is uncertain). The position of these two components in the Hertzsprung-Russell (H-R) diagram is typical of normal O V stars (i.e., neither is particularly close to the ZAMS), although their association with an O3 V primary could be considered an indirect indication of youth.

These examples serve to illustrate the difficulty of trying to understand the O Vz subclass on a case-by-case basis, not helped by the paucity of quantitative information available. To clarify their nature, and their possible links to young (ZAMS) and/or weak-wind stars, analysis of an extensive and homogeneous dataset is needed. Such a dataset is now available from the VLT-FLAMES Tarantula Survey (VFTS, Evans et al. 2011), an ESO Large Program which has obtained multi-epoch spectroscopy of over 800 massive stars in the 30 Doradus (hereafter 30 Dor) star-forming region of the LMC.

Spectral classification of the O-type stars observed in the VFTS has led to the discovery of ~50 O Vz stars in 30 Dor (Walborn et al., in prep.). In this article we undertake quantitative spectroscopic analysis of the apparently single O Vz stars from the VFTS (i.e., stars with constant radial velocities from the multi-epoch spectroscopy, see Sana et al. 2013), together with a control sample of normal O V stars (i.e., without the "z" suffix) from the same survey. With these data, we perform a differential study between the O Vz and O V samples to test if the O Vz stars are (a) younger, (b) subluminous, (c) of higher gravity, and/or (d) have weaker winds than normal O V stars.

In Sect. 2 we present the samples of O V and O Vz stars from the VFTS analyzed in this study. In Sect. 3 we explain the automatic method used to analyze the spectra and note issues which need to be taken into account; our results are presented in Sect. 4. Section 5 presents a theoretical study of the Vz phenomenon with synthetic FASTWIND models, and these predictions are compared with our results in Sect. 6. We end with a discussion and our conclusions in Sect. 7.

2. Observations and sample selection

An introduction to the VFTS, along with an extensive description of the observing strategy and data reduction was presented by Evans et al. (2011). In brief, all of the data considered in this

[1] The number of detected/known O Vz stars in the MW and the Large Magellanic Cloud (LMC) has increased since Walborn's review due to large spectroscopic surveys in the MW (GOSSS, Maíz Apellániz et al. 2012; OWN, Barbá et al. 2010; IACOB, Simón-Díaz et al. 2011a) and the LMC (Evans et al. 2011).

Table 1. Wavelength coverage and resolving power (R) of the FLAMES-Giraffe settings used in the survey.

Setting	Range (Å)	R
LR02	3960–4564	7000
LR03	4499–5071	8500
HR15N	6442–6817	16 000

study were obtained using the Medusa mode of the Fibre Large Array Multi-Element Spectrograph (FLAMES; Pasquini et al. 2002) on the Very Large Telescope (VLT). The Medusa fibres couple light from targets across a 25′ field-of-view on the sky into the Giraffe spectrograph, providing intermediate-resolution spectroscopy of over 130 targets simultaneously.

Three of the standard settings of the Giraffe spectrograph were used: LR02, LR03, and HR15N; the resulting spectral coverage and delivered resolving power (R) of each setting is summarized in Table 1. The same spectra have also been used to provide detailed spectral classifications (Walborn et al., in prep.), and to investigate the multiplicity (Sana et al. 2013) and rotational properties (Ramírez-Agudelo et al. 2013) of the O-type population in 30 Dor.

From the ∼340 O-type stars in the VFTS, Walborn et al. (in prep.) have identified 48 objects which display He II λ4686 absorption that is stronger than any other He line in the blue-violet region, and hence were classified as O Vz. Ten of these were identified by Sana et al. (2013) as showing large-amplitude (i.e., larger than 20 km s^{-1}) radial-velocity variations and were discarded from the sample to avoid possible misinterpretation due to their binary nature. The final sample of O Vz stars considered here therefore comprises 38 (apparently) single stars. These were complemented with a control sample of 46 O V stars from the VFTS, which were selected following the same criteria, i.e., from the total sample of normal O V stars, with those identified as binaries or having uncertain spectral classifications discarded.

The first three columns of Tables A.1–A.3 list the VFTS identifications and spectral classifications (from Walborn et al., in prep.) of the stars considered here. The spectral types range from O2 to O9.5/O9.7 for both samples (see Fig. 1). Interestingly, there seems to be a clear difference in the distribution of spectral types between the samples: the O Vz stars tend to be concentrated at intermediate types (O5.5 – O7), while the O V stars mostly have types later than O8.

Figure 2 shows the spatial distribution of the O Vz and O V samples. Walborn et al. (in prep.) found that the O Vz stars seem to be concentrated within regions of recent and current star formation (i.e., the ionizing clusters NGC 2060 and 2070, as well as an east-west band at the northern edge of the nebula). Walborn et al. also found that the distribution of O Vz stars is quite different to that of the rapidly rotating stars. However, when the spatial distribution of O V and O Vz stars are compared (without any constraint in the rotational velocities) there does not seem to be a clear difference between them.

Figure 3 shows two characteristic Medusa spectra[2], which include suitable diagnostic lines of hydrogen and helium for the quantitative analysis presented in this paper. Given that detected binaries were discarded from the samples, the multi-epoch spectra for each object were combined (after individual normalization) to increase the signal-to-noise (S/N) ratio. In addition, the

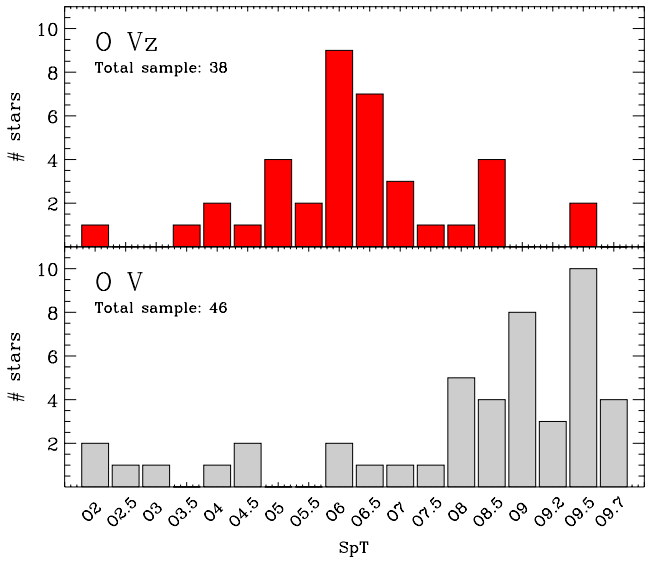

Fig. 1. Distribution of spectral types for the O Vz (red) and O V (gray) stars analyzed.

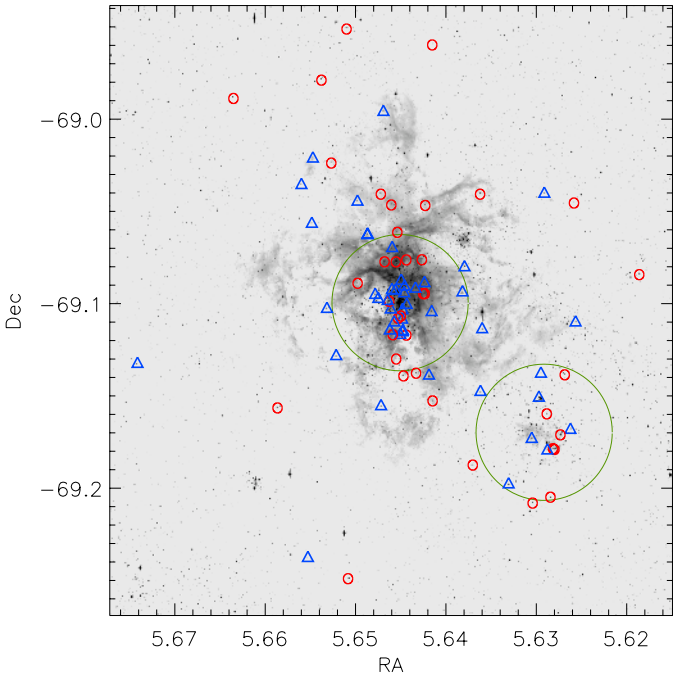

Fig. 2. Spatial distribution of the O Vz (red circles) and O V (blue triangles) stars analyzed in 30 Doradus. The central and south-western green circles indicate the approximate extent of the NGC 2070 and NGC 2060 clusters, respectively.

wavelength scales of the combined spectra were corrected to the rest frame, using the velocities from Sana et al. (2013). The S/N of the combined spectra is typically ∼150 (with 27 cases with $S/N > 200$, and 14 with $S/N < 100$). As illustrated in Fig. 3, nebular lines emitted by the ionized gas are present in all the spectra, contaminating the stellar absorption lines (mainly the hydrogen Balmer and He I lines) to differing degrees. This has important consequences for the accurate determination of the stellar and wind parameters of some of the stars in our sample (see Sect. 3), especially in cases where the nebular emission lines are strong and broad.

[2] We refer the reader to Walborn et al. (in prep.) for further examples of O Vz spectra from the VFTS. Also note that the spectra and best-fitting models for the primary diagnostic lines used in this study are shown in Figs. B.1 to B.3.

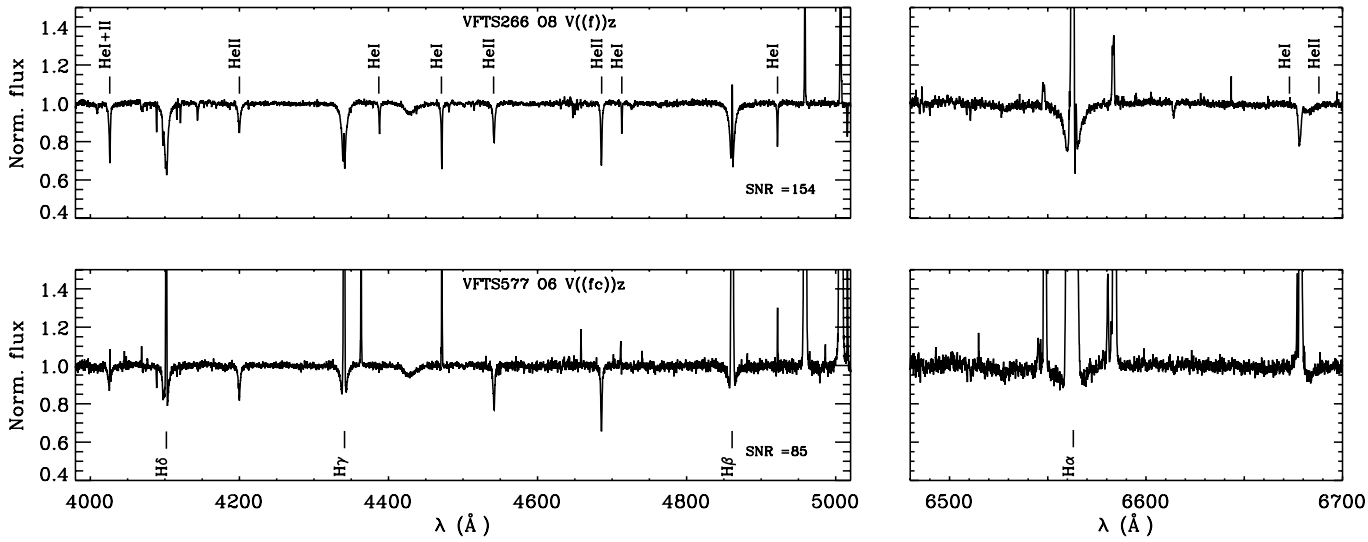

Fig. 3. Two examples of the FLAMES-Medusa spectra used in this study, in which VFTS 577 (*lower panel*) has serious contamination by nebular emission. The diagnostic hydrogen and helium lines used in our analysis are indicated (see Table 3).

3. Quantitative spectroscopic analysis

The stellar parameters of our sample were determined using standard techniques (see e.g., Herrero et al. 1992, 2002; Repolust et al. 2004), employing the FASTWIND stellar atmosphere code (Santolaya-Rey et al. 1997; Puls et al. 2005) and the IACOB-Grid Based Automatic Tool (IACOB-GBAT), a tool developed for automated spectroscopic analysis of O stars.

The tool uses a large grid of FASTWIND models which span a wide range of stellar and wind parameters (which are optimized for the analysis of O-type stars), and uses a χ^2 algorithm to perform comparisons between the observed and synthetic H I, He I, and He II line profiles; a detailed description of the IACOB-GBAT was given by Simón-Díaz et al. (2011b). In this section we comment on some of the details concerning application of the IACOB-GBAT to analysis of the VFTS data.

3.1. Grid of FASTWIND models

From the various FASTWIND grids which are presently incorporated in the IACOB-GBAT, we have considered the models computed for $Z = 0.5\,Z_\odot$, corresponding to the approximate metallicity of the LMC (e.g., Mokiem et al. 2007). The $0.5\,Z_\odot$ grid was constructed assuming six free parameters: effective temperature $T_{\rm eff}$, logarithmic surface gravity $\log g$, helium abundance by number relative to hydrogen Y(He), microturbulence $\xi_{\rm t}$, the exponent of the wind velocity law β, and the wind-strength parameter Q. This parameter was defined by Puls et al. (1996), and it groups the mass-loss rate $\dot{M}$, the terminal velocity v_∞, and the stellar radius R together under the optical-depth invariant $Q = \dot{M}\,(R\,v_\infty)^{-3/2}$. Depending on ρ^2 processes in O and B stars profiles of Hα and other lines are nearly identical for the same Q. Therefore, this is the parameter actually covered by the analysis. Mass-loss rates can only be determined if v_∞ is known (and radius, but this is obtained in our analysis). Unfortunately, v_∞ is not known for our stars. Although we could adopt a calibration (see e.g., Vink et al. 2001) we refrain from it for two reasons: a) it would introduce an unknown error in the mass-loss rate and b) we do not know a priori whether there is a difference in the v_∞ of O V and O Vz stars. Therefore, we stick to Q for the analysis, as this is the parameter derived directly from the spectroscopic analysis. v_∞ would require UV observations of the targets, which is much more expensive in observing time given the limited multiplexing capabilities of the HST.

Table 2. Parameter ranges considered in the FASTWIND grid incorporated in the IACOB-GBAT used in this study.

Parameter	Ranges and/or specific values
Z	$0.5\,Z_\odot$
$T_{\rm eff}$	≥25 000 K [Step: 1000 K]
$\log g$	[2.6–4.3] dex [Step: 0.1 dex]
Y(He) (1)	0.06, 0.09, 0.10, 0.12, 0.15, 0.20, 0.25, 0.30
$\zeta_{\rm t}$ (2)	5, 10, 15, 20 km s^{-1}
$\log Q$	–15.0, –14.0, –13.5, –13.0, –12.7, –12.5, –12.3, –12.1 –11.9, –11.7
β (2)	0.8, 1.0, 1.2, 1.5, 1.8

Notes. (1) Defined as $Y(\mathrm{He}) = N(\mathrm{He})/N(\mathrm{H})$. (2) See, however, notes in Sects. 3.4.1 and 3.4.2.

Our grid of models were computed under the assumption of no clumping. As shown by Najarro et al. (2011), model fits for stars with thin winds (like O V stars in the LMC) require no clumping and therefore, to first order, are probably unclumped. Moreover, as this is a differential analysis, only the difference in behavior of this already weak clumping between O V and O Vz would be relevant. Hence, we consider the use of unclumped models in the study presented here fully justified. A summary of the parameter ranges covered by the grid is given in Table 2.

3.2. Line broadening parameters

As part of the VFTS series of papers, Ramírez-Agudelo et al. (2013) have provided estimates for the projected rotational velocities ($v \sin i$) for the single O-type stars from the survey. Given the objectives and scale of their study, they did not investigate the effects of macroturbulent broadening in their sample, which may be important in the context of the analysis presented here.

We therefore proceeded as follows: we initially used the $v \sin i$ values from Ramírez-Agudelo et al. and checked if the global broadening of the He I-II lines was properly reproduced. In cases with a clear disagreement between the global broadening of the observed and synthetic lines from the best-fitting

Table 3. Hydrogen and helium lines used in the spectroscopic analysis (from the three FLAMES-Medusa settings).

LR02	LR03	HR15N
H_δ (4102)	H_β (4861)	H_α (6563)
H_γ (4341)	He I 4713	He I 6678
He I+II 4026	He I 4922	He II 6683
He I 4387	He II λ4541	
He I λ4471	He II λ4686	
He II 4200		

model, we iterated on the $v \sin i$ value to improve the final fit (in this way, we mimic the effects of macroturbulence).

In addition, we needed to modify the $v \sin i$ values for 17 of the 84 stars analyzed here. Six of these were stars with low $v \sin i$ values for which, as indicated by Ramírez-Agudelo et al., the estimates were less certain given the adopted methods. A further nine cases correspond to stars with $v \sin i \geq 150\,\mathrm{km\,s^{-1}}$ with weak or heavily contaminated He I lines. Finally, we detected two stars with much broader He I lines than He II lines; both stars have close companions in images from the *Hubble* Space Telescope (HST), suggesting that the spectra are composite (see Sect. 4).

3.3. Diagnostic lines

The diagnostic lines used for the stellar parameter determination of our samples of O Vz and O V stars are summarized in Table 3. The same weight was initially given to each line, but the full H I and He I profiles could not be used in many of the stars due to nebular contamination. Note that the fitting strategy followed by the IACOB-GBAT requires all these contaminated regions within the line profiles to be clipped before the analysis.

Nebular hydrogen Balmer lines are present in all the spectra, with H_α the most affected line (see Figs. B.1–B.2). In all cases, while the nebular emission contaminates the cores of H_β, H_γ, and H_δ (to differing extents), the wings of these lines can still provide reliable diagnostics of the stellar gravity. The situation for the H_α line is worse; there is an important fraction of stars for which the whole profile is heavily contaminated. This could impose a challenge in the determination of the wind-strength Q-parameter but, in the case of O-dwarfs (where changes in the wind properties only affect the core of H_α), this issue is mitigated by the inclusion of He II λ4686 in the analysis. As with H_α, He II λ4686 has a strong dependence on the Q-parameter, but is not affected by nebular contamination in our data.

The He I lines are contaminated by nebular emission (to different degrees) in ~70% of the analyzed sample. This is not a significant problem for mid/late O-type stars with $v \sin i$ above a certain value (where the He I lines are strong and broad), but the accuracy (and even reliability) of the analyzes can be affected for narrow-lined and/or early-type stars. Thus, results from the IACOB-GBAT analysis of the stars in which important parts of the He I line profiles were clipped must be handled with care and were carefully checked. As described in the next section, the stellar parameter which can be most affected by nebular contamination of the He I lines is $T_{\rm eff}$, which also produces a secondary effect on $\log g$ and Y(He).

3.4. Stellar parameter determination

The strategy followed by the IACOB-GBAT for the determination of the stellar parameters is based on the minimization of the quantity $\chi^2_{\rm T}$ (as described by Simón-Díaz et al. 2011b), which is a measurement of the global goodness-of-fit of a given synthetic spectrum to the observed data. The investigation of how this quantity varies with the different stellar and wind parameters of interest (i.e., $\chi^2_{\rm T}$ distributions) provides an objective and homogeneous determination of the best values and associated uncertainties of the parameters under study, and also identifies cases where a given parameter cannot be properly constrained (or if only upper/lower limits can be determined).

Before discussing the general strategy followed for the cases of $T_{\rm eff}$, $\log g$, Y(He), and $\log Q$, we present below some notes on the results for the β-parameter and the microturbulence.

3.4.1. β-parameter

The FASTWIND grid was computed for six values of the β-parameter, but initial tests with β as a free parameter indicated that the $X^2_{\rm T}$ distributions were degenerate, i.e., β cannot be constrained for the stars analyzed in this paper. Therefore, we adopted $\beta = 0.8$, a typical value for O-type dwarfs (see, e.g., Repolust et al. 2004), and predicted by theory including a finite disk and multiple scattering (Müller & Vink 2008). This approach reduces the computational time required for the analysis of each star down to about 5–20 min, depending on the specific case.

3.4.2. Microturbulence

We also found that the $\chi^2_{\rm T}$ distribution for microturbulence is degenerate in many cases, with others indicating a somewhat smaller $\chi^2_{\rm T}$ (i.e., better fit) for a microturbulence of $5\,\mathrm{km\,s^{-1}}$. We therefore concluded that microturbulence cannot be adequately constrained for the stars in this study and adopted $\xi_{\rm t} = 5\,\mathrm{km\,s^{-1}}$ in our analysis. While the value may be higher in the case of mid and early O dwarfs, consideration of other values would only vary the final parameters within the standard error box (see also Villamariz & Herrero 2000).

3.4.3. $T_{\rm eff}$, $\log g$, Y(He), and $\log Q$

In general, we were able to provide estimates (plus associated formal errors) for these four parameters for most of the analyzed stars. However, we also found some cases in which we could only provide upper/lower limits, and detected a few stars for which a quantitative spectroscopic analysis based exclusively on the H and He lines could not provide reliable estimates of the effective temperature. Some notes on how we dealt with these situations are described below.

Figure 4 shows some illustrative examples of the $\chi^2_{\rm T}$ distributions resulting from the IACOB-GBAT analysis of stars in our sample. Panels (a) to (c) can be considered as typical examples of distributions from which the associated parameter could be properly determined. The distributions are symmetric and clearly peaked around a central value. In a situation like this, we use the fitting curve of the lower envelope of the distribution to provide the central value and associated 1σ uncertainties.

For almost half of the stars in the sample we obtained a $\chi^2_{\rm T}$ distribution in $\log Q$ similar to the one presented in Fig. 4e. This is mainly a result of the fact that below a certain value of the mass-loss rate, both H_α and He II λ4686 become insensitive to changes in the Q-parameter. This effect is aggravated by the presence of nebular lines contaminating the core of the H_α line. In such cases, we could provide upper limits for $\log Q$, given by

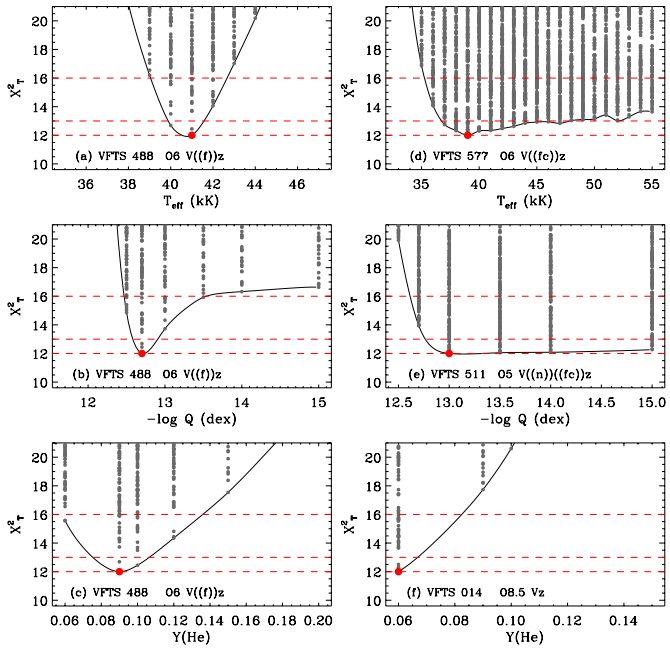

Fig. 4. Examples of χ^2_T distributions from the IACOB-GBAT analysis. From top to bottom, $T_{\rm eff}$, $\log Q$ and Y(He). Horizontal dashed red lines correspond to the minimum χ^2_T value and the associated 1σ and 2σ deviating limits from the best-fitting model (computed as $\chi^2_{T,min}$ + 1 and $\chi^2_{T,min}$ + 4, respectively). Black curves result from a smooth fit to the lower envelope of each distribution.

the intersection of the fitting curve of the lower envelope of the distribution with the 1σ (horizontal) limits.

We also proceeded in a similar way in situations such as the example presented in Fig. 4f, where the minimum of the distribution is found at the grid boundary. This only occurred in a few cases, for which we could only provide upper limits for the helium abundance. We suggest that the low abundances found in these cases (4 O Vz and 9 O V) could be a consequence of either the presence of undetected companions that would dilute the He lines in the global spectrum (resulting in lower Y(He) abundances than expected), or the limitations in the analysis because of low S/N, strong nebular contamination or even weak He I lines.

Finally, Fig. 4d shows a distribution that questions the possibility to provide a reliable estimation of $T_{\rm eff}$ for this specific case. While there is a clear minimum in the distribution, the degeneracy is quite remarkable below the 2σ level. Even if only those models with value of χ^2_T below the 1σ limit are considered, an uncertainty in $T_{\rm eff}$ of ~5000 K is obtained following the strategy described above. This situation mainly occurs for stars in which an important fraction of the He I line profiles are contaminated by nebular emission and/or the He I lines are weak/absent. In such cases, the He I/He II ionization balance (the main diagnostic of $T_{\rm eff}$) is difficult to determine, and only very rough temperature estimates could be obtained. As a consequence, results for the other three parameters (especially $\log g$ and Y(He)) must be handled with care.

As mentioned in Sect. 3.3, roughly 70% of the stars in the analyzed sample present some degree of nebular contamination of the He I lines (see Figs. B.1–B.2). After checking each case, we found that the situation is not critical for most objects, and the only consequence is larger uncertainties. However, for about a dozen stars, mainly concentrated at the earliest spectral types, it was not possible to provide robust stellar parameters based exclusively on a HHe analysis (these are discussed further below).

4. Results

Results from the quantitative analysis of our sample, based on their H and He profiles, are presented in Tables A.1 (O Vz) and A.2 (O V). As indicated above, there are a few objects where the reliability of the $T_{\rm eff}$ estimates was doubtful as sufficient He I lines were not available for analysis. These stars are excluded from Tables A.1 and A.2, and will be analyzed separately using an approach similar to that described by Rivero González et al. (2012), which employs N III-V lines as the primary $T_{\rm eff}$ diagnostic. Complete results of these HHeN analyzes, including estimates of nitrogen abundances, will be presented by Simón-Díaz et al. (in prep.). For completeness, for these 13 stars, we provide first estimates of the stellar and wind parameters of interest for this study in Table A.3.

The column entries in Tables A.1 and A.2 are as follows: (1) VFTS identifier; (2, 3) spectral classification from Walborn et al. (in prep.); (4) absolute visual magnitude M_V, computed from the extinction-corrected, apparent V magnitudes from Maíz Apellániz et al. (in prep.) and for a distance modulus of 18.5 (Gibson 2000); (5) $v \sin i$ considered in the analysis; (6−13) derived effective temperature, gravity, helium abundance and wind-strength Q-parameter, and their estimated uncertainties (more specifically, the formal errors); (14) stellar luminosity, obtained from M_V and following the procedure outlined by Kudritzki & Puls (2000) and Herrero et al. (1992); (15) comments from Walborn et al. regarding possible binarity/multiplicity. The entries in Table A.3 are similar, but without the formal uncertainties given the preliminary nature of the results.

As indicated in Table A.1, we have adopted a minimum value of 0.1 dex for the $\log g$ formal errors, since we consider that uncertainties below this value are not realistic. There are several error sources to take into account besides those coming from the systematics of the method, such as the continuum renormalization (see, e.g., Castro et al. 2012).

These tables are complemented with a series of figures (Figs. B.1−B.3) in which the best-fitting synthetic spectra are overplotted on the observed data for the most important diagnostic lines for this study, i.e., H_γ, He I λ4471, He II λ4541, He II λ4686, and H_α.

These results have been used to investigate the hypotheses introduced in Sect. 1 regarding the nature of the O Vz stars. We especially emphasize that this investigation is based on a differential analysis comparing results from a homogeneous analysis of the O Vz and O V objects within our sample. To inform our discussion, we have plotted our data in three different diagrams: $\log g$ vs. $T_{\rm eff}$, $\log Q$ vs. $T_{\rm eff}$ and the H-R diagram (i.e., $\log L/L_\odot$ vs. $T_{\rm eff}$), as shown in Figs. 6–8, respectively. In these figures, the red and black symbols represent the O Vz and O V stars, respectively. Stars with results from the HHeN analysis (i.e., from Table A.3) are plotted with diamonds, and the open squares in Figs. 6 and 8 correspond to the stars with close visual companions. Finally, the stars for which only an upper limit in $\log Q$ could be established (see notes in Sect. 3.4) are plotted in Fig. 7 as open circles, with associated downward arrows.

To compare with the predictions of the evolutionary models, in Figs. 6 and 8 we also plot evolutionary tracks (solid green lines), the ZAMS (solid black line), and isochrones (dotted gray lines, for ages up to 6 Myr) from Brott et al. (2011), calculated

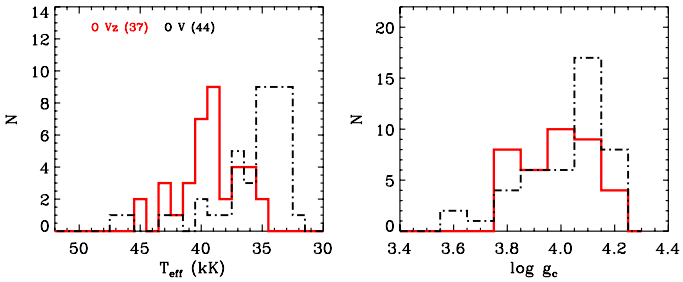

Fig. 5. Distribution of effective temperatures and gravities (corrected for rotation) for the O Vz and O V stars (dot-dashed red and black lines, respectively). The three O2-type stars discussed in Sect. 4 are not included due to their likely composite nature.

for the metallicity of the LMC and an initial rotational velocity[3] of 171 km s^{-1}.

At this point, we note that while performing the HHeN analysis of the three O2 stars in our sample (VFTS 468, 506, and 621), we found that their Medusa spectra display weak (but clearly detectable) He I absorption. The FASTWIND models do not predict the detection of these lines for the effective temperatures derived from the N IV/N V ionization balance. This result, together with the clear detection of multiple visual components within the 1.2″ Medusa fibres for two of them, warns us about the interpretation of results for these stars as single objects. These three stars were therefore omitted from the figures and are not discussed further. Also omitted are five stars for which photometric data were not available (indicated in Tables A.1–A.3 by a dash in the M_V and $\log L/L_\odot$ columns).

4.1. Effective temperatures and gravities

We start by considering three of the stellar parameters which are directly obtained from the spectroscopic analysis, namely $T_{\rm eff}$, $\log g$, and $\log Q$. Here we concentrate on the first two, while the wind properties of the analyzed stars are discussed in next section. Figure 5 shows the general distribution of O V and O Vz stars in these two parameters. As expected from their distribution in spectral types (see Fig. 1), the two samples present a distinct distribution in temperature, with O Vz and O V stars dominating at intermediate and low temperatures, respectively. The two distributions overlap in a transition region spanning $35\,000 \lesssim T_{\rm eff} \lesssim 40\,000$ K. A small but similar number of objects of both types are found with $T_{\rm eff} \geq 45\,000$ K. The peculiar relative $T_{\rm eff}$ distributions of the Vz and V stars suggests that effective temperature plays an important role in the Vz phenomenon.

Though intriguing, this is not necessarily incompatible with the postulated nature of the O Vz stars. On the contrary, the comparison of the distributions in gravity challenges the statement that these objects should have higher gravities than normal O dwarfs due to their hypothesized proximity to the ZAMS. The range of gravities covered by both types of objects is similar. Moreover, contrary to expectations, the distribution is almost flat for the O Vz stars, but peaked towards higher gravities for the O V stars. Thus, O Vz stars do not especially have higher gravities when compared to normal O dwarfs.

Figure 6 compares the distribution of our results in the $\log g$ vs. $\log T_{\rm eff}$ plane. At first inspection, the figure confirms the two results presented above, but also shows that the O V z stars do not appear particularly closer to the ZAMS (in terms of gravity) than the normal O dwarfs. This distribution cannot be reconciled with the expectations, even taking into account the uncertainties in the derived gravities (up to 0.2 dex in a few cases, but with a median value of ∼0.13 dex).

Interestingly, three temperature zones can be distinguished in our results (illustrative limits between these are indicated by the vertical dashed lines in Figs. 6 to 8):

- Zone 1 ($T_{\rm eff} \leq 35\,000$ K), where only O V stars are found;
- Zone 2 ($40\,000 \leq T_{\rm eff} \leq 35\,000$ K), where there are similar numbers of O Vz and O V stars. Although both types of objects cover a similar range in gravity, O Vz stars tend to concentrate at lower gravities and higher effective temperatures than normal O dwarfs;
- Zone 3 ($T_{\rm eff} \geq 40\,000$ K), where the number of O Vz stars dominates. Only a few O V stars are found at relatively low gravities (3.9–3.7 dex), while the range of gravities covered by O Vz stars ranges from 4.2 to 3.8 dex.

The unexpected distribution of stars in Fig. 6 will be investigated further in Sect. 5, taking into account FASTWIND predictions concerning the relative behavior of the three main diagnostic lines involved the Vz classification (i.e., He I λ4471, He II λ4541, and He II λ4686).

As an aside, we note the recent warning from Massey et al. (2013) about gravities derived using FASTWIND models (v10.1). Massey et al. presented a comparison of CMFGEN (Hillier & Miller 1998) and FASTWIND results, finding a difference of ∼0.1 dex between the derived gravities (in which lower gravities are found from the FASTWIND analyzes). This warns us about the use of $\log g$ vs. $\log T_{\rm eff}$ to infer stellar ages and masses. However, as we are presenting a differential analysis based on results from the same code and techniques, our conclusions regarding the properties of O Vz stars should not be affected.

4.2. Wind properties

To investigate the wind properties of the analyzed sample, we present the derived $\log Q$ values as a function of the effective temperature in Fig. 7. From inspection of their location in this figure, one could conclude that the O Vz stars are concentrated at the lower envelope of the distribution (i.e., they have weaker winds). However, it is also interesting to have a closer look at the wind properties of both samples in the three temperature zones described in Sect. 4.1.

It is particularly remarkable that, although a similar range in $\log Q$ is found in the three zones (especially below 42 000 K), the relative distribution of $\log Q$ values for both types of objects is clearly dependent on the range of effective temperatures considered:

- Zone 1: the Vz characteristic is not present in any stars, even in those for which low $\log Q$ values were obtained;
- Zone 2: except for a few O V stars with values of $\log Q$ above −12.7, there is no clear correlation in this region between wind strength and O Vz/O V classification. Intriguingly, there are a fair number of stars identified as O V with similar wind strengths (or upper limits in $\log Q$) compared to some of the O Vz stars;
- Zone 3: although the O V stars generally have higher $\log Q$ values than the O Vz stars, it is interesting that there are a few O Vz stars with relatively large $\log Q$ estimates (in terms of the range of values measured for the whole sample).

[3] Selected from the model grid of initial rotational velocities as the closest to the average $v \sin i$ in our sample.

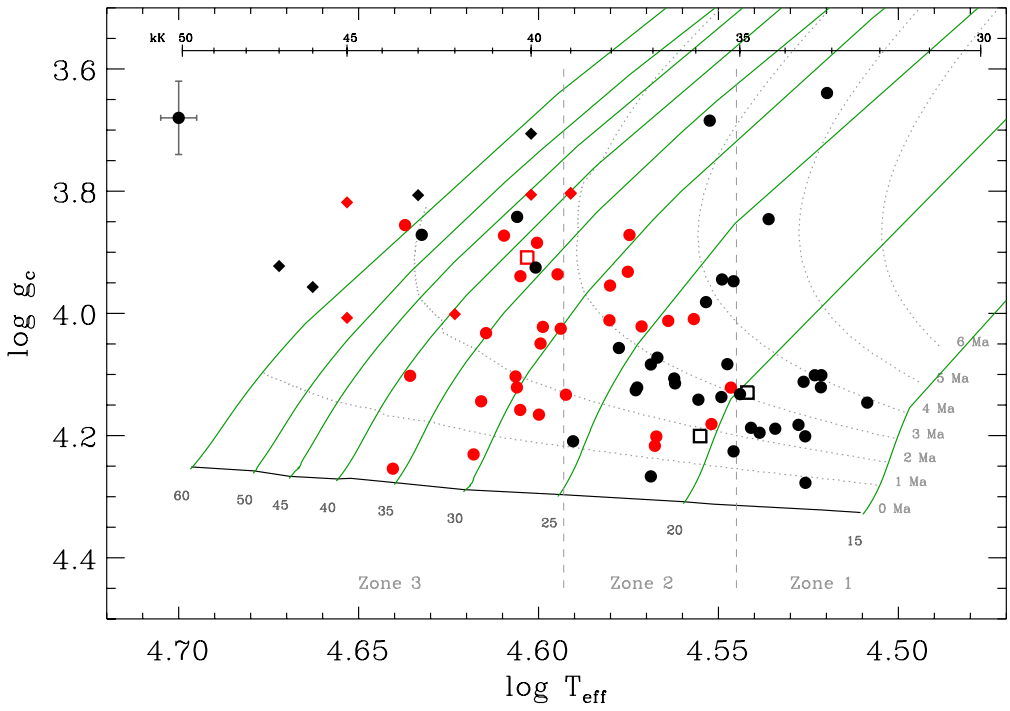

Fig. 6. $\log g$ vs. $\log T_{\rm eff}$ results for the O Vz and O V samples (red and black symbols, respectively). Objects with confirmed close companions in the Medusa fibres (see footnote to Table A.1) are plotted as open squares. Stars analyzed using nitrogen lines are indicated with diamonds. To aid the discussion, the diagram has been divided into three temperature zones (see text for details).

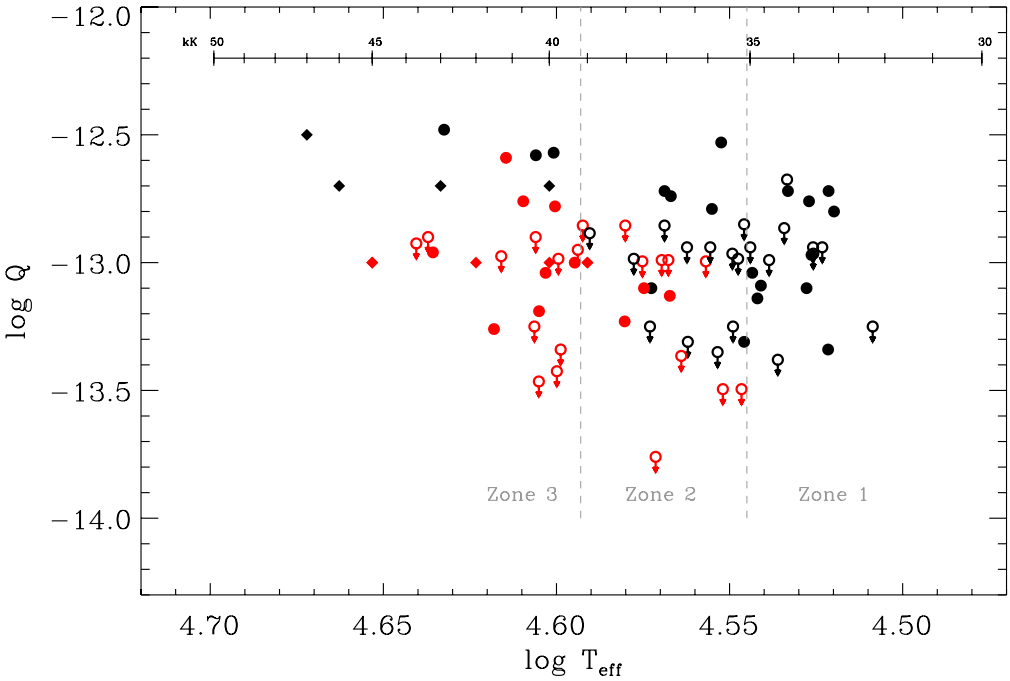

Fig. 7. $\log Q$ vs. $\log T_{\rm eff}$ results for the O V z and O V samples (red and black symbols, respectively). Cases where there was degeneracy in the $\chi^2_{\rm T}$ distributions used to determine $\log Q$ are indicated as upper limits (with downward arrows). Stars analyzed using nitrogen lines are indicated with diamonds. As in Fig. 6, the diagram has been divided into three temperature zones.

Therefore, although wind strength seems to play a role in the occurrence of the Vz classification (as expected), there seems to be another factor involved, especially in the Zone 2 temperature range.

We would like to point out here that UV observations (in the spectral range 1100–1800 Å) could help to better constrain the wind properties of those stars for which only upper limits have been obtained. This spectral range contains some lines which are more sensitive to wind variations than Hα and He II λ4686, especially in the weak wind regime.

4.3. Luminosities and ages

As the star evolves away from the ZAMS towards lower temperatures, its gravity decreases and its stellar luminosity increases, so its wind strength is also expected to increase. Since the intensity of the He II λ4686 line depends strongly on this parameter (see Sect. 1), it is predicted that O stars evolving from the ZAMS should lose their Vz characteristic.

A first view of the H-R diagram for the stars (Fig. 8) indicates that the lower envelope of the distribution (with respect to the ZAMS) is dominated by the O Vz stars, while the O V objects concentrate in the upper envelope. Therefore, one could conclude that, as a group, the O Vz stars in 30 Dor are younger and less luminous (in an evolutionary sense) than the O V stars. However, a more detailed inspection (see also Table 4) indicates the presence of a non-negligible, unexpected number of O Vz objects at relatively advanced ages (between 2 and 4 Myr) and ten O V stars similarly close to the ZAMS (below the 2 Myr isochrone) as some of the O Vz stars.

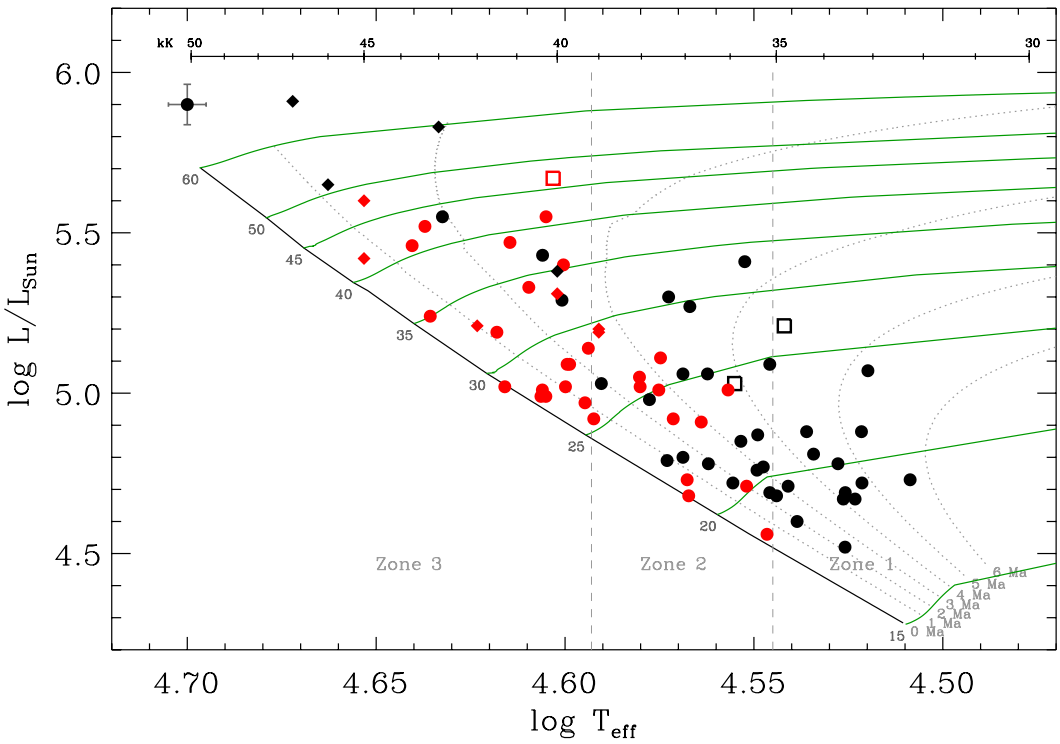

Fig. 8. Hertzsprung-Russell diagram for O Vz and O V samples (red and black symbols, respectively). The other symbols are the same as those used in Fig. 6, together with the same three temperature zones.

Table 4. Number of O Vz and O V stars in different age ranges and temperature zones as estimated using the evolutionary tracks from Brott et al. (2011) with an initial rotation rate of 171 km s^{-1} (see Fig. 8).

	Zone 1		Zone 2		Zone 3		Total	
Age	O Vz	O V	O Vz	O V	O Vz	O V	O Vz	O V
<1 Myr	0	0	4	1	7	0	11	1
1–2 Myr	0	1	1	4	8	4	9	9
2–3 Myr	0	2	7	3	7	3	14	8
3–4 Myr	0	1	2	9	0	0	2	10
>4 Myr	0	11	0	1	0	0	0	12
Total	0	15	14	18	22	7	36	40

The latter feature can likely be explained by the rotational velocities of the stars. Most of the O V stars below the 2 Myr isochrone (computed from models with an *initial* $v \sin i$ of 171 km s^{-1}) actually have $v \sin i > 200$ km s^{-1}, and so they could be somewhat more evolved objects. However, the large relative number of O Vz to O V stars with inferred ages of between 2 and 4 Myr is more challenging to understand.

The three temperature zones described in Sect. 4.1 are also indicated in Fig. 8. Interestingly, the O Vz and O V stars in Zone 2 cover a similar range in luminosity, i.e., stars of both types can be found having similar temperatures and luminosities. The O V stars in Zone 3 are mainly concentrated at higher luminosities, but we also find O Vz stars in this luminosity regime; this seems to indicate that other parameters/effects apart from age and luminosity may play a role in the O Vz phenomenon.

When interpreting results from the H-R diagram, the effects of visually undetected binaries (or physically unrelated, close companions) on the measured photometry (hence the derived luminosity) should be considered. VFTS 096 is an example of an O Vz star with an erroneous luminosity (plotted as a red open square in Fig. 8). Inspection of the HST/WFC3 images revealed a nearby companion of similar brightness within the 1.2″ fibre aperture. Due to their proximity, the two objects were not resolved in the ground-based images used to obtain the photometry and, as a consequence, the star appears to be overluminous when compared with other objects with similar $T_{\rm eff}$ and $\log g$ (e.g., VFTS 601 and 746).

We have checked for similar cases among the O Vz stars located above the 2 Myr isochrone and found that VFTS 096 is the only one with a clear detection of nearby objects which may significantly influence the measured photometry[4]. Even if we assume that VFTS 096 only contributes half of the estimated luminosity, it would still be located far away from the ZAMS (well above the 2 Myr isochrone). Therefore, although it cannot be completely ruled out, we consider it very improbable that unresolved companions can explain the relatively large number of O Vz stars with ages above 2 Myr. A more likely explanation, related to the dependence of the wind strength with metallicity, is presented in Sect. 5.

4.4. Summary of results from the analysis

In summary, the analysis of our sample of 38 O Vz and 46 O V stars in 30 Dor leads to the following main conclusions:

1. There do not appear to be significant differences in the derived gravities of the O Vz and O V stars. In particular, the O Vz stars do not concentrate at higher gravities relative to normal O dwarfs.
2. The O Vz stars tend to be closer to the ZAMS than O V stars, but we have also found a non-negligible number further away (with ages of 2–4 Myr).
3. As a group, the O Vz stars tend to define the lower envelope of luminosities and wind strengths, but they are also found over the full range of values obtained for normal O V stars.
4. As expected, wind strength is an important parameter to be taken into account for the understanding of the

[4] VFTS 110 and 398 also have close companions in the HST/WFC3 images. However, in both cases the *visual companion* is significantly fainter and so the expected effect on m_v is almost negligible.

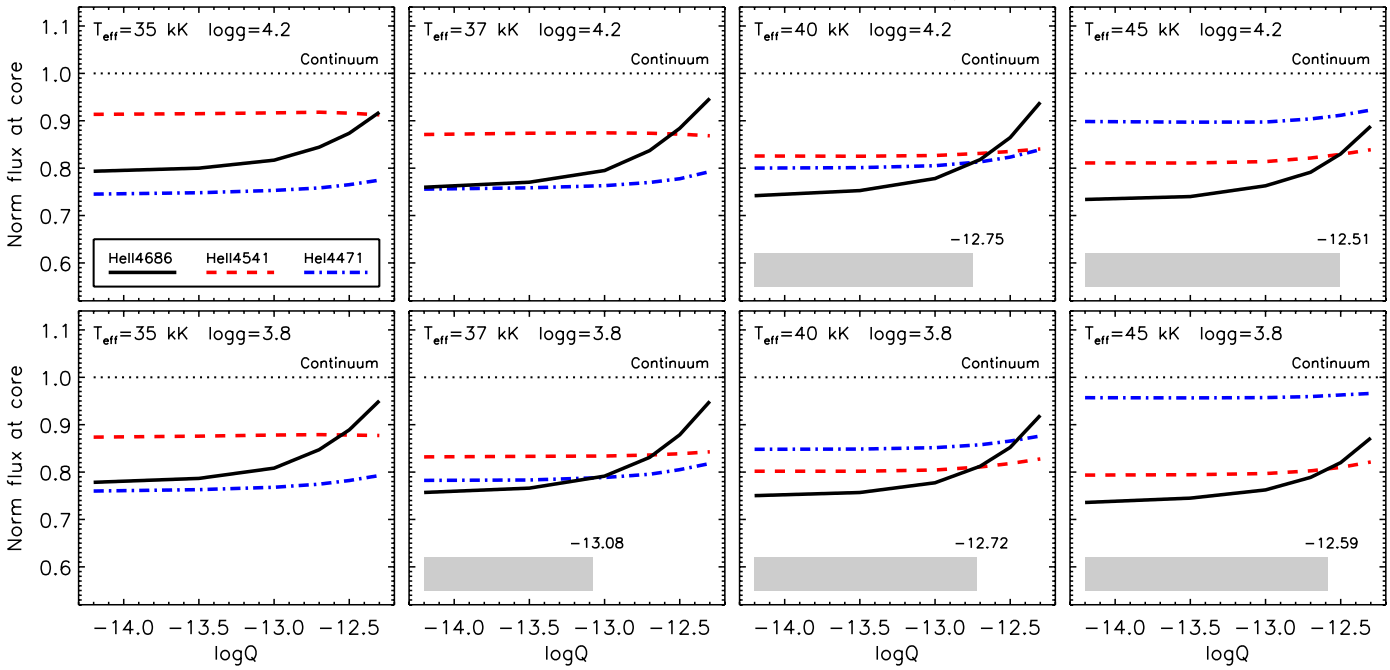

Fig. 9. FASTWIND predictions of the behavior of the lines involved in the Vz phenomenon (He I λ4471, He II λ4541 and He II λ4686) as a function of the wind-strength Q-parameter for different ($T_{\rm eff}$, $\log g$) pairs. A fixed projected rotational velocity ($v \sin i = 100\,{\rm km\,s^{-1}}$) and resolution ($R = 8000$) have been considered. The range of $\log Q$ values for which a star would be classifed as a Vz star are indicated with the gray rectangle. The corresponding upper $\log Q$ value leading to the Vz characteristic is also quoted.

Vz phenomenon. In addition, the distinct temperature distribution found for the O Vz and O V samples indicates that $T_{\rm eff}$ is the second key parameter. Also, the overlapping ranges of stellar parameters of both types of objects in the range $35\,000 \leq T_{\rm eff} \leq 40\,000$ K point towards one or more additional parameters playing a role.

5. The Vz phenomenon as predicted by FASTWIND models

In this section, we use synthetic spectra from the grid of FASTWIND models to investigate the predicted effect of several spectroscopic parameters in the occurrence of the Vz characteristic. In particular, we concentrate on effective temperature, gravity, wind strength and projected rotational velocity.

5.1. Behaviour of the relevant He lines

An O dwarf is classified as Vz when He II λ4686 is stronger in absorption than both He I λ4471 and He II λ4541. We therefore focussed the FASTWIND predictions on these three lines. Figure 9 shows the variation of the normalized central intensities for the three lines as a function of $\log Q$, for representative ($T_{\rm eff}$, $\log g$) pairs, which span the range of our results in 30 Dor (see Figs. 6 and 7). In particular, we have considered four $T_{\rm eff}$ values and two $\log g$ values (organized in columns and rows, respectively). The synthetic lines were degraded to the resolving power of the VFTS Medusa spectra ($R = 8000$), and convolved with a rotational broadening profile corresponding to $v \sin i = 100\,{\rm km\,s^{-1}}$. We initially fixed $v \sin i$ to this value for simplicity in the discussion; further investigation of the effect of rotational broadening on the Vz characteristic is discussed in Sect. 5.2.

As expected, while there is a strong dependence of the depth of the He I λ4471 and He II λ4541 lines with $T_{\rm eff}$ (and to a lesser extent, $\log g$), these lines are almost insensitive to variations in the wind strength (at the values corresponding to O dwarfs). In contrast, the flux at the core of He II λ4686 is only somewhat affected by changes in $T_{\rm eff}$ and $\log g$, but varies strongly with $\log Q$. These plots also allow us to illustrate why it is only possible to provide upper limits for the wind-strength parameter in a large fraction of the analyzed stars: below a certain value of $\log Q$ (between –13.0 and –13.5) the depth of He II λ4686 remains unaffected. A similar effect also occurs for Hα, the other (main) wind diagnostic line in the optical spectral range.

As indicated above, the Vz characteristic is defined as He II λ4686 line being deeper than He II λ4541 and He I λ4471. In Fig. 9 this translates to the solid black curve in a given panel being below the dashed red and dash-dotted blue lines. The range in $\log Q$ where this occurs for a given ($T_{\rm eff}$, $\log g$) pair is indicated with a gray rectangle. The two main conclusions which can be extracted from inspection of these figures are:

- Below a given $T_{\rm eff}$ (which depends on the gravity) the Vz characteristic never occurs. He I λ4471 is always stronger in absorption than He II λ4686 due to the low temperature of the star, independent of the wind strength.
- At higher temperatures there is a certain $\log Q$ value below which the star would be classified as Vz. This upper limit in the wind-strength parameter seems to increase with temperature (i.e., stars with higher temperatures require higher $\log Q$ values to lose their Vz characteristic), and also depends on $\log g$ for a given $T_{\rm eff}$.

The combined dependencies of the Vz characteristic on $T_{\rm eff}$, $\log g$ and $\log Q$ are shown in a more compact way in Fig. 10. The boundaries in $\log Q$ between the regions where O Vz and O V stars would be expected (below and above the lines, respectively) are plotted as a function of $T_{\rm eff}$, for $v \sin i = 100\,{\rm km\,s^{-1}}$

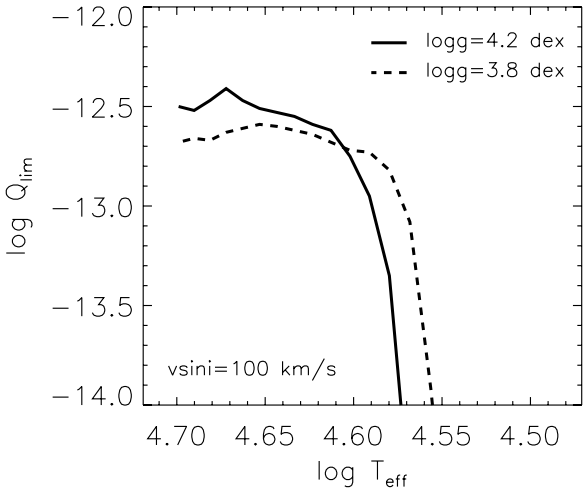

Fig. 10. Upper limits in the Q-parameter, as a function of $T_{\rm eff}$, below which Vz objects are expected (for $v \sin i = 100\,{\rm km\,s^{-1}}$ and two different values of $\log g$).

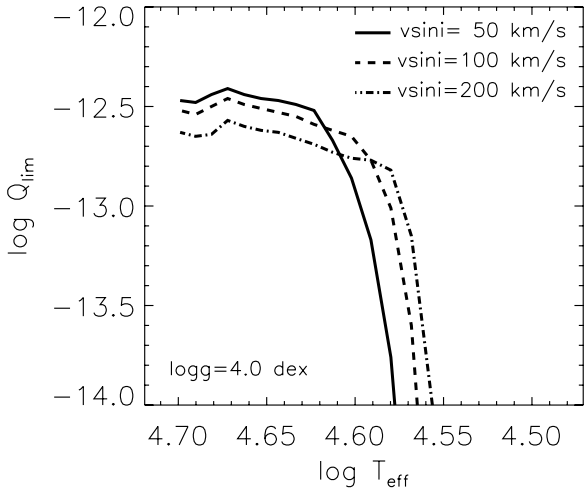

Fig. 11. Same as Fig. 10 but for $\log g = 4.0$ dex and three different values of $v \sin i$.

and two $\log g$ values. The two curves vary similarly with $T_{\rm eff}$, characterized by a strong dependence of $\log Q_{\rm lim}$ at intermediate temperatures, and an almost flat region above a certain value (i.e., the boundary in $\log Q$ becomes almost insensitive to temperature). In addition, the curve for $\log g = 4.2$ is shifted to somewhat higher temperatures and $\log Q$ values compared to $\log g = 3.8$.

Therefore, in addition to wind strength, the effective temperature and gravity of the star are two important parameters to be taken into account to interpret the Vz phenomenon from an evolutionary point of view. This may be especially important in the range of temperatures where there is a strong dependence of $Q_{\rm lim}$ with $T_{\rm eff}$ and $\log g$. For example, a star with $T_{\rm eff} = 38\,000$ K ($\log T_{\rm eff} = 4.58$), $v \sin i = 100\,{\rm km\,s^{-1}}$ and $\log Q = -12.8$ (an intermediate value for the 30 Dor sample, see Fig. 7) would be classified as V if $\log g = 4.2$, and as Vz if $\log g = 3.8$. Note that the star with $\log g = 4.2$ dex would still be classified as O V, even if the wind strength is much lower. While this example contradicts what might be expected from an evolutionary point of view, it can be explained by taking into account the relative dependencies of the three diagnostic lines with $T_{\rm eff}$, $\log g$, and $\log Q$.

In Sect. 6 we discuss the implications of the FASTWIND predictions on the interpretation of our results for the samples in 30 Dor in more detail. However, we first investigate a fourth important parameter, the rotational broadening ($v \sin i$).

5.2. The role of rotational broadening on the Vz phenomenon

Rotational broadening is expected to influence the depths of the He I and He II lines differently (e.g., Markova et al. 2011). As the Vz classification is based on the relative depths of He I λ4471, He II λ4541, and He II λ4686, we also investigated the influence that rotation may have on its occurrence.

In Fig. 11 we plot a similar comparison to that shown in Fig. 10, but now for a fixed gravity and three different $v \sin i$ values. The curves in the figure confirm an important influence of rotational broadening, which is comparable in impact to that of the gravity (although with different causes). In particular, the region in which there is a strong dependence of the $Q_{\rm lim}$ boundary with $T_{\rm eff}$, moves to lower $T_{\rm eff}$ with increasing $v \sin i$.

We conclude that higher values of $v \sin i$ generally favor the presence of O Vz stars at relatively low temperatures (below $T_{\rm eff} \sim 38\,000$ K), with the opposite effect in the high $T_{\rm eff}$ regime (where a lower $\log Q$ value is required to lose the Vz characteristic).

This result can be easily understood taking into account the different (relative) effect that rotational broadening produces on the three diagnostic lines. In particular, one should remember that intrinsic Stark broadening in the He I line is quadratic, while it is linear in the He II lines (and that the intrinsic width of He II λ4541 is slightly broader than He II λ4686). The narrower the line, the more it is affected by rotational broadening. This explains why, at relatively low temperatures (when He I λ4471 is stronger in absorption than the other two He II lines), rotation favors the Vz characteristic for a given value of $\log Q$. At higher temperatures, when the important diagnostic lines in the definition of the Vz phenomenon are He II λ4541 and He II λ4686, the effect works in the opposite direction.

5.3. Summary of FASTWIND predictions

To sum up, the main conclusions from the FASTWIND model predictions concerning the Vz characteristic are:

1. Wind strength and effective temperature are the key parameters in understanding the Vz phenomenon. However, other parameters such as gravity and projected rotational velocity are also important in defining the occurrence of this characteristic for a given wind strength and temperature.
2. At low temperatures ($T_{\rm eff} \lesssim 35\,000$ K) only O V stars are expected, independent of the wind strength. The temperature is not sufficiently high for He II λ4686 to be stronger in absorption than He I λ4471, even for very low values of $\log Q$.
3. At intermediate temperatures ($35\,000 \lesssim T_{\rm eff} \lesssim 40\,000$ K) occurrence of the Vz characteristic for a given value of $\log Q$ strongly depends on the specific values of $T_{\rm eff}$, $\log g$ and $v \sin i$. In this region, FASTWIND models predict that high gravities and low $v \sin i$ values favor the presence of normal O V stars, even for objects with relatively low values of $\log Q$. The relative fraction of Vz to V stars in this region is expected to increase towards the upper limit in $T_{\rm eff}$.
4. At high temperatures ($T_{\rm eff} \gtrsim 40\,000$ K) the boundary in $\log Q$ between O Vz and O V stars becomes almost insensitive to $T_{\rm eff}$, and relatively high values of $\log Q$ are needed to make

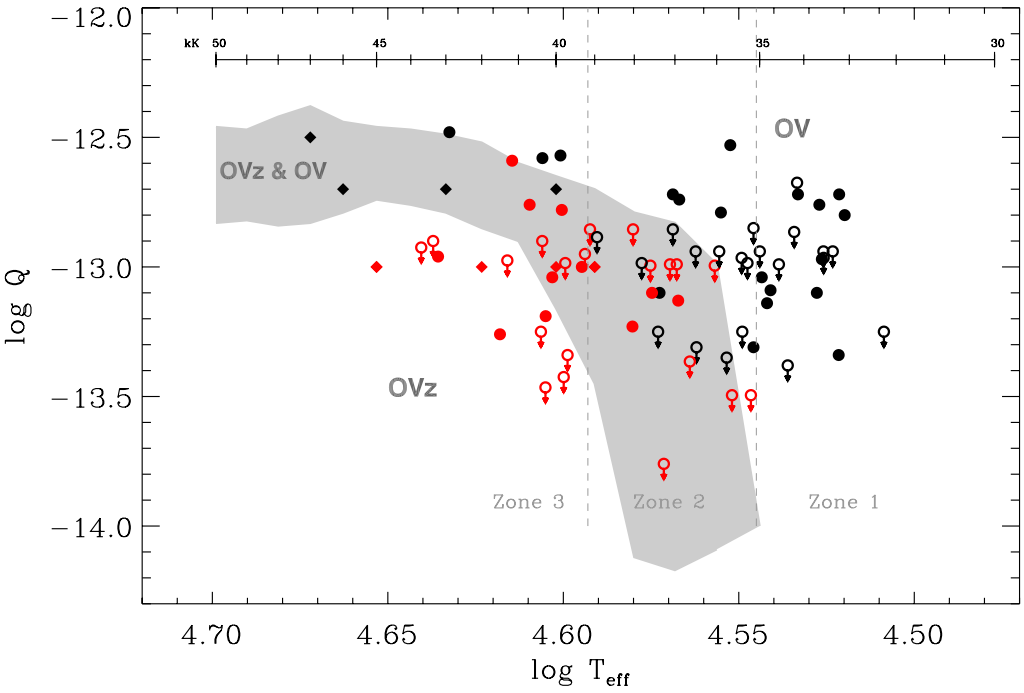

Fig. 12. FASTWIND predictions for Vz behavior with $\log Q$ as a function of $T_{\rm eff}$, for models with $3.8 \leq \log g \leq 4.2$ dex, and $50 \leq v \sin i \leq 300$ km s^{-1}, compared to the results from our analyses with the IACOB-GBAT. The shaded area indicates the region where we expect both O Vz and O V stars from our analysis (see text), whereas we expect only O V/O Vz stars above/below this area. Symbols as used in Fig. 7.

a star of a given $T_{\rm eff}$ lose its Vz characteristic. In this region, high gravities and low $v \sin i$ values favor the presence of Vz stars.

6. The Vz phenomenon: observations vs. model atmosphere predictions

Our investigation of the O Vz phenomenon as predicted by the FASTWIND models allows us to further interpret the results from our analysis of the O Vz and O V samples in 30 Dor.

In the previous section we have shown that the $\log Q$ vs. $\log T_{\rm eff}$ diagram provides a useful way to illustrate the predicted dependence of the occurrence of the Vz phenomenon on $T_{\rm eff}$, $\log g$, $\log Q$ and $v \sin i$. In Fig. 12 we combine our results for the O Vz and O V stars in 30 Dor, with the information extracted from the FASTWIND model predictions. This figure is similar to Fig. 7, but now includes the gray shaded area, which indicates the region where both Vz and V stars are expected (depending on the specific values of $\log g$ and $v \sin i$). The boundaries of the shaded area were obtained from the $Q_{\rm lim}$ values contained in curves such as those in Figs. 10 and 11 (for $3.8 \leq \log g \leq 4.2$ and $50 \leq v \sin i \leq 300$ km s^{-1}). Below/above this area, only O Vz/O V stars are expected.

The first thing to remark on in Fig. 12 is the excellent agreement between the V or Vz classification of the analyzed stars and the FASTWIND predictions. Clean samples of O V and O Vz stars are found above and below the shaded region (respectively), but there is a mixture of both types of objects within that region.

With this figure in mind (as well as Figs. 10 and 11) we can revisit the distribution of O Vz and O V stars in the $\log g$ vs. $\log T_{\rm eff}$ and H-R diagrams (Figs. 6 and 8, respectively). It is now clear why no O Vz stars are found in Zone 1, while the dominance of O Vz stars in Zone 3 can be understood by taking into account that most of the O dwarfs in 30 Dor do not have a strong enough wind to break the Vz characteristic (likely a consequence of the low metallicity of the LMC). Finally, the strong dependence of the Vz characteristic on the specific combination of $T_{\rm eff}$, $\log g$, $\log Q$, and $v \sin i$ for stars with $35\,000 \lesssim T_{\rm eff} \lesssim 40\,000$ K, explains the mixture of O Vz and O V stars found in Zone 2.

It is also interesting to realize that the unexpected distribution of gravities for the objects in Zone 2 (e.g., Fig. 6) may be explained by taking into account the FASTWIND predictions. In Sect. 4.1 it was noted that O Vz stars in this zone tend to concentrate at lower gravities than normal O dwarfs (see Fig. 6). This result is, in some sense, expected from the fact that FASTWIND models predict that high gravities favor the presence of O V stars in this range of temperatures, even for relatively low values of $\log Q$ (see Fig. 10).

We therefore conclude that the global distribution of O Vz and O V stars in 30 Dor in the $\log g$ vs. $\log T_{\rm eff}$, $\log Q$ vs. $\log T_{\rm eff}$, and H-R ($\log L$ vs. $\log T_{\rm eff}$) diagrams (and even most of the unexpected cases) can be explained as a natural combination of stellar parameters. Similar arguments will likely be applicable to the variety of results for O Vz stars in the literature (see notes in Sect. 1).

7. Summary and conclusions

The O Vz stars, a subclass of the O-type dwarfs characterized by having He II λ4686 stronger in absorption than any other He line in their blue-violet spectra, have been suggested to be stars on or near the ZAMS (Walborn 2009). In particular, there are empirical arguments that O Vz stars are younger and subluminous, with higher gravities and weaker winds, when compared to normal O dwarfs. These properties would make O Vz stars of considerable interest to advance our knowledge of the physical properties of massive stars in the very first stages of their lives, an active research field which is still open to debate.

The VFTS has provided a unique opportunity to investigate the proposed hypotheses about the nature of the O Vz stars in more detail. This is because of the large number of O Vz stars discovered in 30 Dor, combined with the excellent quality (in terms of resolving power, S/N ratio, and spectral coverage), homogeneity, and multi-epoch nature of the VFTS data. This has

enabled us to perform a comprehensive quantitative analysis of a statistically-meaningful sample of (very likely single) O Vz and O V stars in the same star-forming region for the first time.

The ultimate goal of this work was to investigate the postulated different (younger) evolutionary stage of O Vz stars in comparison with normal O dwarfs. To address this, we obtained the stellar and wind parameters of a sample of 38 O Vz stars (plus a control sample of 46 O V stars) in 30 Dor by means of standard techniques, using the FASTWIND stellar atmosphere code and the IACOB-GBAT, a grid-based tool developed for automated quantitative analysis of optical spectra of O stars. The derived parameters have been located in three diagrams of interest, namely the $\log g$ vs. $\log T_{\rm eff}$, $\log Q$ vs. $\log T_{\rm eff}$ and H-R diagrams, which have been used to investigate if the O Vz stars have lower luminosities, higher gravities, and weaker winds than the O V stars, and if they are also closer to the ZAMS (i.e., younger), in the frame of a differential analysis.

From inspection of these diagrams we conclude that O Vz stars do not have higher gravities, but they define the lower envelope of the distribution of stars in the H-R and $\log Q$ vs. $\log T_{\rm eff}$ diagrams (i.e., are generally younger and have weaker winds[5] than normal O dwarfs). However, we have also found some results that seem to challenge the postulated nature of the O Vz stars: (a) not all O Vz stars in our sample are less luminous and younger than O V stars with the same spectral types; (b) there is a non-negligible number of O Vz stars with relatively advanced ages (of 2−4 Myr); and (c) at intermediate temperatures (between approx. 35 000 and 40 000 K) there is not a clear correlation between wind strength and Vz (or V) nature. We note that these findings agree with the diversity of results found by other authors in O Vz stars within the Galaxy and the SMC (see Sect. 1).

Interestingly, the two samples have distinct distributions in temperature/spectral type. The O Vz stars concentrate at intermediate and high temperatures, while lower temperatures are dominated by the O V stars. In addition, we have found that the relative distribution of gravities, luminosities, and wind-strength in both types of objects depends on the effective temperature considered. This result indicates that other parameters, apart from wind strength and effective temperature, play a secondary role in the occurrence of the Vz characteristic (such as gravity, luminosity and rotational velocity). As a consequence of the interpretation of the Vz phenomenon in terms of proximity to the ZAMS (i.e., age), it is more complex than initially expected. We should also keep in mind that because rotational broadening has important effects on the way that massive stars evolve away from the ZAMS, two O dwarfs located at the same place in the H-R diagram could actually correspond to two different evolutionary phases.

These findings are confirmed by FASTWIND predictions of the relative behavior (as a function of $T_{\rm eff}$, $\log g$, $\log Q$, and $v \sin i$) of the three main diagnostic lines which define the Vz subclass. This has allowed us to identify the importance of considering the specific combination of these four parameters (in addition to the location of the star in the H-R diagram) for a more complete understanding of the nature of the O Vz phenomenon from an evolutionary point of view. This is especially critical for stars with effective temperatures between 35 000 and 40 000 K. In this temperature range, a star with a modest (or even low) wind strength will appear as O Vz or O V depending on the specific values of $T_{\rm eff}$, $\log g$, and $v \sin i$. In particular, we have shown that lower gravities and higher projected rotational velocities favor the occurrence of the Vz characteristic for a given value of $\log Q$ at intermediate temperatures.

Other predictions of interest are: (a) below ∼35 000 K, He I λ4471 always dominates in absorption over He II λ4686 due to the low temperature of the star; as a consequence, no O Vz stars are expected to be found at these temperatures, even if the star has a weak wind; (b) above ∼40 000 K, the boundary in $\log Q$ between O Vz and O V stars becomes almost insensitive to $T_{\rm eff}$, and relatively high values of $\log Q$ are needed to make a star of a given $T_{\rm eff}$ lose its Vz characteristic. In this region, high gravities and low $v \sin i$ values favor the presence of Vz stars.

The comparison of results from the spectroscopic analysis and the FASTWIND predictions has shown that the distribution of our O Vz and O V stars in the $\log g$ vs. $\log T_{\rm eff}$, $\log Q$ vs. $\log T_{\rm eff}$, and H-R diagrams can be naturally explained as a combination of stellar parameters. However, one should also keep in mind that, as indicated by Walborn et al. (in prep.), the high binary frequency of the O stars might provide an alternative origin for some O Vz spectra: composite spectra of (morphologically normal) early and late O-type dwarfs may produce an apparent mid O Vz morphology.

We propose an explanation to the surprisingly large number of O Vz stars found in 30 Dor, and why some of them are found an unexpectedly large distance away from the ZAMS (above the 2 Myr isochrone). Our hypothesis refers to metallicity: the low metal content of the region implies that most of the O-dwarfs in 30 Dor do not have a wind strong enough to break the Vz characteristic, even in slightly evolved stars. Following from this, a lower percentage of Vz stars might be expected to be found away from the ZAMS in the Galaxy (due to the greater metallicity). In any case, while it seems that some are not ZAMS objects, the O Vz stars remain important objects to be considered in the investigation of the physical properties of the very early phases of massive stars in the Universe.

Acknowledgements. C.S.-S.J., S.S.-D. and A.H. acknowledge financial support from the Spanish Ministry of Economy and Competitiveness (MINECO) under grants AYA2010-21697-C05-04, Consolider-Ingenio 2010 CSD2006-00070 and Severo Ochoa SEV-2011-0187, and by the Canary Islands Government under grant PID2010119. F.N. and M.G. acknowledge support by the Spanish MINECO under grants AYA2010-21697-C05-01 and FIS2012-39162-C06-01. STScI is operated by the Association of Universities for Research in Astronomy, Inc., under NASA contract NAS 5-26555. J.M.A. acknowledges support from the Spanish Government Ministerio de Educación y Ciencia through grants AYA2010-15081 and AYA2010-17631 and the Consejería de Educación of the Junta de Andalucía through grant P08-TIC-4075. The publication is supported by the Austrian Science Fund (FWF).

References

Barbá, R. H., Gamen, R., Arias, J. I., et al. 2010, in Rev. Mex. Astron. Astrofis. Conf. Ser., 38, 30
Bernasconi, P. A., & Maeder, A. 1996, A&A, 307, 829
Bouret, J.-C., Lanz, T., Hillier, D. J., et al. 2003, ApJ, 595, 1182
Bouret, J.-C., Lanz, T., Martins, F., et al. 2013, A&A, 555, A1
Brott, I., de Mink, S. E., Cantiello, M., et al. 2011, A&A, 530, A115
Castro, N., Urbaneja, M. A., Herrero, A., et al. 2012, A&A, 542, A79
Churchwell, E. 2002, ARA&A, 40, 27
Evans, C. J., Taylor, W. D., Hénault-Brunet, V., et al. 2011, A&A, 530, A108
Gibson, B. K. 2000, Mem. Soc. Astron. It, 71, 693
Hanson, M. M. 1998, in Properties of Hot Luminous Stars, ed. I. Howarth, ASP Conf. Ser., 131, 1
Herrero, A., Kudritzki, R. P., Vilchez, J. M., et al. 1992, A&A, 261, 209
Herrero, A., Puls, J., & Najarro, F. 2002, A&A, 396, 949
Heydari-Malayeri, M., Rosa, M. R., Schaerer, D., Martins, F., & Charmandaris, V. 2002, A&A, 381, 951
Hillier, D. J., & Miller, D. L. 1998, ApJ, 496, 407

[5] We note that, given our limitations to determine the wind strength below a certain threshold, this does not confirm nor reject a possible relation between some O Vz stars and the weak-wind stars.

Kudritzki, R.-P., & Puls, J. 2000, ARA&A, 38, 613
Lucy, L. B. 2010, A&A, 524, A41
Mahy, L., Nazé, Y., Rauw, G., et al. 2009, A&A, 502, 937
Mahy, L., Gosset, E., Sana, H., et al. 2012, A&A, 540, A97
Maíz Apellániz, J., Pellerin, A., Barbá, R. H., et al. 2012, in Proceedings of a Scientific Meeting in Honor of Anthony, F. J. Moffat, eds. L. Drissen, C. Rubert, N. St-Louis, & A. F. J. Moffat, ASP Conf. Ser., 465, 484
Markova, N., Puls, J., Scuderi, S., Simón-Díaz, S., & Herrero, A. 2011, A&A, 530, A11
Markova, N., Puls, J., Simón-Díaz, S., et al. 2014, A&A, 562, A37
Martins, F., Schaerer, D., Hillier, D. J., et al. 2005, A&A, 441, 735
Martins, F., Mahy, L., Hillier, D. J., & Rauw, G. 2012, A&A, 538, A39
Mason, B. D., Gies, D. R., Hartkopf, W. I., et al. 1998, AJ, 115, 821
Massey, P., Neugent, K. F., Hillier, D. J., & Puls, J. 2013, ApJ, 768, 6
Mokiem, M. R., de Koter, A., Evans, C. J., et al. 2006, A&A, 456, 1131
Mokiem, M. R., de Koter, A., Evans, C. J., et al. 2007, A&A, 465, 1003
Morrell, N. I., Walborn, N. R., & Fitzpatrick, E. L. 1991, PASP, 103, 1049
Muijres, L. E., Vink, J. S., de Koter, A., Müller, P. E., & Langer, N. 2012, A&A, 537, A37
Müller, P. E., & Vink, J. S. 2008, A&A, 492, 493
Najarro, F., Hanson, M. M., & Puls, J. 2011, A&A, 535, A32
Parker, J. W., Garmany, C. D., Massey, P., & Walborn, N. R. 1992, AJ, 103, 1205
Parker, J. W., Zaritsky, D., Stecher, T. P., Harris, J., & Massey, P. 2001, AJ, 121, 891
Pasquini, L., Avila, G., Blecha, A., et al. 2002, The Messenger, 110, 1
Puls, J., Kudritzki, R.-P., Herrero, A., et al. 1996, A&A, 305, 171
Puls, J., Urbaneja, M. A., Venero, R., et al. 2005, A&A, 435, 669
Ramírez-Agudelo, O. H., Simón-Díaz, S., Sana, H., et al. 2013, A&A, 560, A29
Repolust, T., Puls, J., & Herrero, A. 2004, A&A, 415, 349
Rivero González, J. G., Puls, J., Massey, P., & Najarro, F. 2012, A&A, 543, A95
Sana, H., de Koter, A., de Mink, S. E., et al. 2013, A&A, 550, A107
Santolaya-Rey, A. E., Puls, J., & Herrero, A. 1997, A&A, 323, 488
Simón-Díaz, S., Castro, N., Garcia, M., & Herrero, A. 2011a, in IAU Symp. 272, eds. C. Neiner, G. Wade, G. Meynet, & G. Peters, 310
Simón-Díaz, S., Castro, N., Herrero, A., et al. 2011b, J. Phys. Conf. Ser., 328, 012021
Villamariz, M. R., & Herrero, A. 2000, A&A, 357, 597
Vink, J. S., de Koter, A., & Lamers, H. J. G. L. M. 2001, A&A, 369, 574
Walborn, N. R. 1973, ApJ, 179, 517
Walborn, N. R. 2009, in Massive stars: from Pop III and GRBs to the Milky Way, eds. M. Livio, & E. Villaver, STScI Symp. Ser., 20, 167
Walborn, N. R., & Blades, J. C. 1997, ApJS, 112, 457
Walborn, N. R., & Parker, J. W. 1992, ApJ, 399, L87
Zinnecker, H., & Yorke, H. W. 2007, ARA&A, 45, 481

Pages 15 to 24 are available in the electronic edition of the journal at http://www.aanda.org

Appendix A: Tables

Tables A.1 and A.2 present the stellar parameters from our HHe analysis of the O Vz and O V samples. Table A.3 presents first estimates for the stars where it was also necessary to use nitrogen lines in the analysis due to weak He I lines and/or strong nebular contamination.

Table A.1. Stellar and wind parameters obtained from quantitative analysis of our sample of O Vz stars.

VFTS	SpT	LC	M_v[1]	$v \sin i$ [kms^{-1}]	$T_{\rm eff}$ [K]	$\Delta T_{\rm eff}$ [K]	$\log g$ [dex]	$\Delta \log g$[2] [dex]	$\log g_{\rm c}$[3] [dex]	Y(He)[4]	$\log Q$ [dex]	$\Delta \log Q$ [dex]	$\log L/L_\odot$[5] [dex]	Comments[6]
355	O4	V((n))((fc))z	–5.1	135	43 400	600	3.84	0.10	3.85	0.09	<–12.9	–	5.52	NC
418	O5	V((n))((fc))z	–4.4	135	43 200	1700	4.09	0.13	4.10	0.09	–13.0	0.3	5.24	SB?
511	O5	V((n))((fc))z	–4.9	105	43 700	1700	4.25	0.11	4.25	0.10	<–12.9	–	5.46	SB1s
398	O5.5	V((n))((f))z	–5.1	65	41 200	1000	4.03	0.10	4.03	<0.06	–12.6	0.2	5.47	SBvs
601	O5-6	V((n))z	–5.4	125	40 300	500	3.93	0.10	3.94	0.09	–13.2	0.4	5.55	...
096	O6	V((n))((fc))z	–5.7	125	40 100	500	3.90	0.10	3.91	0.09	–13.0	0.2	5.67	SBvs VM2
110	O6	V((n))z	–5.0	150	39 900	1000	3.86	0.10	3.88	<0.06	–12.8	0.2	5.40	VM2?
117	O6:	Vz	–4.1	75	41 300	1500	4.14	0.16	4.14	0.12	<–13.0	–	5.02	SB?
356	O6:	V(n)z	–4.5	215	39 300	1300	3.99	0.13	4.03	0.10	<–13.0	–	5.14	SB?
470	O6:	V((f))z	–4.1	75	39 300	600	3.93	0.10	3.94	0.10	–13.0	0.5	4.97	...
472	O6	Vz	–4.1	40	40 400	900	4.12	0.12	4.12	0.11	<–12.9	–	5.01	...
488	O6	V((f))z	–4.8	55	40 700	700	3.87	0.10	3.87	0.09	–12.8	0.2	5.33	...
536	O6	Vz	–4.4	40	41 500	1500	4.23	0.15	4.23	0.09	–13.3	0.6	5.19	SB?
089	O6.5	V((f))z Nstr	–4.3	50	39 700	700	4.02	0.12	4.02	0.13	<–13.3	–	5.09	...
123	O6.5	Vz	–4.0	65	40 400	700	4.10	0.12	4.10	0.13	<–13.3	–	4.99	SB?
549	O6.5	Vz	–4.3	110	39 800	1200	4.04	0.16	4.05	0.09	<–13.0	–	5.09	SB?
761	O6.5	V((n))((f))z Nstr	–4.1	110	40 300	700	4.15	0.10	4.16	0.18	<–13.5	–	4.99	NC
380	O6-7	Vz	–3.9	65	39 100	700	4.13	0.10	4.13	<0.09	<–12.9	–	4.92	...
392	O6-7	V((f))z	–4.5	40	37 600	800	3.87	0.10	3.87	0.10	–13.1	0.2	5.11	...
706	O6-7	Vnnz	–4.2	375	38 000	1200	3.80	0.13	3.95	0.11	<–12.9	–	5.02	...
722	O7	Vnnz	–4.1	405	36 600	800	3.84	0.10	4.01	0.11	<–13.4	–	4.91	SB? NC
724	O7	Vnnz	–4.3	370	37 600	3300	3.78	0.41	3.93	0.19	<–13.0	–	5.01	NC
849	O7	Vz	–4.1	95	39 800	600	4.16	0.11	4.17	0.11	<–13.4	–	5.02	NC
751	O7-8	Vnnz	–4.4	360	36 000	1500	3.90	0.25	4.01	0.10	<–13.0	–	5.01	NC
266	O8	V((f))z	–4.3	40	38 000	500	4.01	0.10	4.01	0.10	–13.2	0.3	5.05	...
014	O8.5	Vz	–	90	37 100	600	3.91	0.10	–	<0.06	<–13.0	–	–	SBs
168	O8.5	Vz	–4.1	40	37 300	500	4.02	0.10	4.02	0.10	<–13.8	–	4.92	SB?
252	O8.5	Vz	–3.6	100	37 000	500	4.21	0.10	4.22	0.11	<–13.0	–	4.73	...
638	O8.5	Vz	–3.5	45	36 900	500	4.20	0.10	4.20	0.10	–13.1	0.3	4.68	...
067	O9.5	Vz	–3.3	40	35 000	1100	4.12	0.19	4.12	0.08	<–13.5	–	4.56	SB?
132	O9.5	Vz	–3.6	40	35 600	700	4.18	0.10	4.18	0.10	<–13.5	–	4.71	...

Notes. [(1)] Values taken from Maíz Apellániz et al. (in prep); the estimated average uncertainties are $\Delta M_V = 0.3$, accounting for uncertainties in the distance modulus (see Gibson 2000) and the apparent magnitudes. [(2)] Formal errors adopting a minimum value of 0.1 dex. [(3)] $\log g_{\rm c} = \log [g + (v \sin i)^2/R_*]$ (see Herrero et al. 1992; Repolust et al. 2004). [(4)] ΔY(He) = 0.02. [(5)] The combined uncertainties in M_V and $T_{\rm eff}$ (from the IACOB-GBAT analysis) lead to an estimated average error in luminosity of $\Delta \log L/L_\odot = 0.13$ dex. [(6)] Relevant comments from Table 1 of Walborn et al. (in prep.): SB, spectroscopic binary; 1, single lined; 2, double lined; s, small amplitude (10–20 km s^{-1}); vs, very small amplitude (<10 km s^{-1}); SB?, stellar absorption displaced from nebular emission lines but no radial-velocity variation measured; SB2?, confirmed SB with possible second companion or unconfirmed SB but two companions visible in the line-of-sight; VMn, visual multiple of n components within the 1.2″ Medusa fibre, as determined from HST/WFC3 images; NC, no WFC3 coverage.

Table A.2. Stellar and wind parameters obtained from quantitative analysis of our sample of O V stars.

VFTS	SpT	LC	M_v[1]	$v \sin i$ [kms^{-1}]	$T_{\rm eff}$ [K]	$\Delta T_{\rm eff}$ [K]	log g [dex]	Δlog g^2 [dex]	log $g_{\rm c}$[3] [dex]	Y(He)[4]	log Q [dex]	Δlog Q [dex]	log $L/L_\odot$[5] [dex]	Comments[6]
385	O4-5	V((n))((fc))	–5.2	120	42 900	1700	3.86	0.10	3.87	0.09	–12.5	0.2	5.55	SBs
491	O6	V((fc))	–5.1	50	40 400	800	3.84	0.08	3.84	0.10	–12.6	0.2	5.43	SB?
746	O6	Vnn	–4.8	275	39 900	1200	3.86	0.10	3.92	0.08	–12.6	0.2	5.29	...
484	O6-7	V((n))	–5.4	120	35 700	700	3.67	0.10	3.68	<0.07	–12.5	0.2	5.41	...
770	O7	Vnn	–4.2	350	37 800	1100	3.95	0.15	4.06	0.10	<–13.0	–	4.98	...
285	O7.5	Vnnn	–3.9	600	35 300	900	3.63	0.10	4.08	0.14	<–13.0	–	4.77	...
065	O8	V(n)	–3.8	165	37 100	1100	4.06	0.16	4.08	0.10	<–12.9	–	4.80	...
249	O8	Vn	–3.8	300	36 500	800	4.04	0.11	4.11	0.10	<–13.3	–	4.78	...
494	O8	V(n)	–4.2	230	38 900	1700	4.20	0.23	4.21	0.09	<–12.9	–	5.03	SB2?
611	O8	V(n)	–3.8	210	37 400	900	4.09	0.14	4.13	0.10	<–13.3	–	4.79	...
768	O8	Vn	–4.7	290	35 100	1200	3.88	0.18	3.95	0.10	–13.3	0.6	5.09	SB2? NC
130	O8.5	V((n))	–4.5	170	36 500	1330	4.09	0.19	4.11	0.08	<–12.9	–	5.06	...
154	O8.5	V	–5.0	55	37 400	700	4.12	0.13	4.12	0.09	–13.1	0.3	5.30	SBs
361	O8.5	V	–5.0	70	36 900	700	4.07	0.10	4.07	<0.06	–12.7	0.1	5.27	...
597	O8-9	V(n)	–4.1	210	35 400	700	3.90	0.11	3.94	0.11	<–13.3	–	4.87	...
074	O9	Vn	–3.7	265	35 100	1300	4.18	0.21	4.23	0.10	<–12.9	–	4.69	...
138	O9	Vn	–3.5	350	34 600	900	4.10	0.14	4.20	0.10	<–13.0	–	4.60	SB2?
280	O9	V((n))	–4.2	150	34 400	600	3.82	0.10	3.85	0.10	<–13.4	–	4.88	...
419	O9:	V(n)	–4.8	145	33 100	900	3.61	0.10	3.64	0.14	–12.8	0.2	5.07	...
483	O9	V	–	40	33 700	900	4.09	0.11	–	0.11	–12.8	0.2	–	SB?
493	O9	V	–4.4	200	37 100	1000	4.25	0.10	4.27	<0.08	–12.7	0.2	5.06	...
521	O9	V(n)	–5.0	150	34 800	600	4.12	0.10	4.13	0.09	–13.1	0.2	5.21	VM2
892	O9	V	–4.0	40	35 800	600	3.98	0.10	3.98	0.11	<–13.4	–	4.85	NC
250	O9.2	V((n))	–3.9	155	35 400	805	4.12	0.15	4.14	0.09	<–13.0	–	4.76	SB?
704	O9.2	V(n)	–	240	34 200	1500	3.98	0.22	–	0.09	<–12.7	–	–	SB?
775	O9.2	V	–3.7	40	35 900	1300	4.14	0.20	4.14	0.12	<–12.9	–	4.72	SB? NC
149	O9.5	V	–3.7	125	35 000	1400	4.12	0.24	4.13	0.12	<–12.9	–	4.68	...
498	O9.5	V	–4.3	40	33 200	800	4.12	0.15	4.12	0.09	–13.3	0.5	4.88	...
560	O9.5	V	–3.3	40	33 600	1200	4.20	0.16	4.20	0.09	<–12.9	–	4.52	...
582	O9.5	V((n))	–	115	35 000	800	4.27	0.10	–	<0.08	–13.0	0.3	–	...
592	O9.5	Vn	–3.7	295	33 600	1000	4.23	0.13	4.28	<0.10	<–13.0	–	4.69	...
649	O9.5	V	–3.7	105	34 800	600	4.18	0.10	4.19	0.09	–13.1	0.2	4.71	...
660	O9.5	Vnn	–4.0	515	32 300	1000	3.95	0.16	4.15	0.11	<–13.3	–	4.73	...
677	O9.5	V	–4.4	40	35 900	1100	4.20	0.13	4.20	<0.07	–12.8	0.2	5.03	VM3
679	O9.5	V	–3.9	40	33 200	900	4.10	0.15	4.10	<0.07	–12.7	0.2	4.72	SB?
778	O9.5	V	–4.0	125	34 200	1400	4.20	0.22	4.19	0.09	<–12.9	–	4.81	...
369	O9.7	V	–3.7	40	33 400	1200	4.10	0.18	4.10	<0.09	<–12.9	–	4.67	...
554	O9.7	V	–	45	34 100	800	4.26	0.10	–	<0.07	–12.7	0.2	–	...
627	O9.7	V	–3.7	50	33 600	600	4.11	0.12	4.11	0.10	–13.0	0.3	4.67	...
639	O9.7	V	–4.0	65	33 700	500	4.18	0.10	4.18	0.09	–13.1	0.2	4.78	SB?

Notes. [(1),(2),(3),(4),(5),(6)] See corresponding notes to Table A.1.

Table A.3. First estimates of stellar and wind parameters from HHeN analysis of the subsample of stars for which He I-II analysis alone was considered unreliable (see notes in Sect. 4).

VFTS	SpT	LC	$M_v^{(1)}$	$v \sin i$ [kms^{-1}]	$T_{\rm eff}$ [K]	$\log g$ [dex]	$\log g_c^{(3)}$ [dex]	$\log Q$	$\log L/L_\odot{}^{(5)}$ [dex]	Comments$^{(6)}$
468	O2	V((f*))+OB	–6.1	80	52 000	4.20	4.20	–12.3	6.17	VM4
506	ON2	V((n))((f*))	–6.6	100	55 000	4.20	4.20	–12.5	6.43	SB1s
621	O2	V((f*))z	–6.1	80	54 000	4.20	4.20	–12.7	6.22	VM3
169	O2.5	V(n)((f*))	–5.8	200	47 000	3.90	3.92	–12.5	5.91	SB?
755	O3	Vn((f*))	–5.2	285	46 000	3.90	3.94	–12.7	5.65	...
797	O3.5	V((n))((fc))z	–5.2	140	45 000	3.80	3.82	–13.0	5.60	SB?
216	O4	V((fc))	–5.9	100	43 000	3.80	3.81	–12.7	5.83	SB?
586	O4	V((n))((fc))z	–4.7	100	45 000	4.00	4.01	–13.0	5.42	SB?
382	O4-5	V((fc))z	–4.8	75	40 000	3.80	3.81	–13.0	5.31	...
581	O4-5	V((fc))	–5.0	70	40 000	3.70	3.71	–12.7	5.38	...
537	O5	V((fc))z	–4.6	60	39 000	3.80	3.80	–13.0	5.19	...
550	O5	V((fc))z	–4.6	50	39 000	3.80	3.80	–13.0	5.20	...
577	O6	V((fc))z	–4.4	40	42 000	4.00	4.00	–13.0	5.21	...

Notes. $^{(1)(3)(5)(6)}$ See corresponding notes in Table A.1.

Appendix B: Figures

Figures B.1 to B.3 show the best-fitting models to the observed VFTS spectra for the most important diagnostic lines in this study, i.e., H_γ, He I λ4471, He II 4541, He I 4686, and H_α.

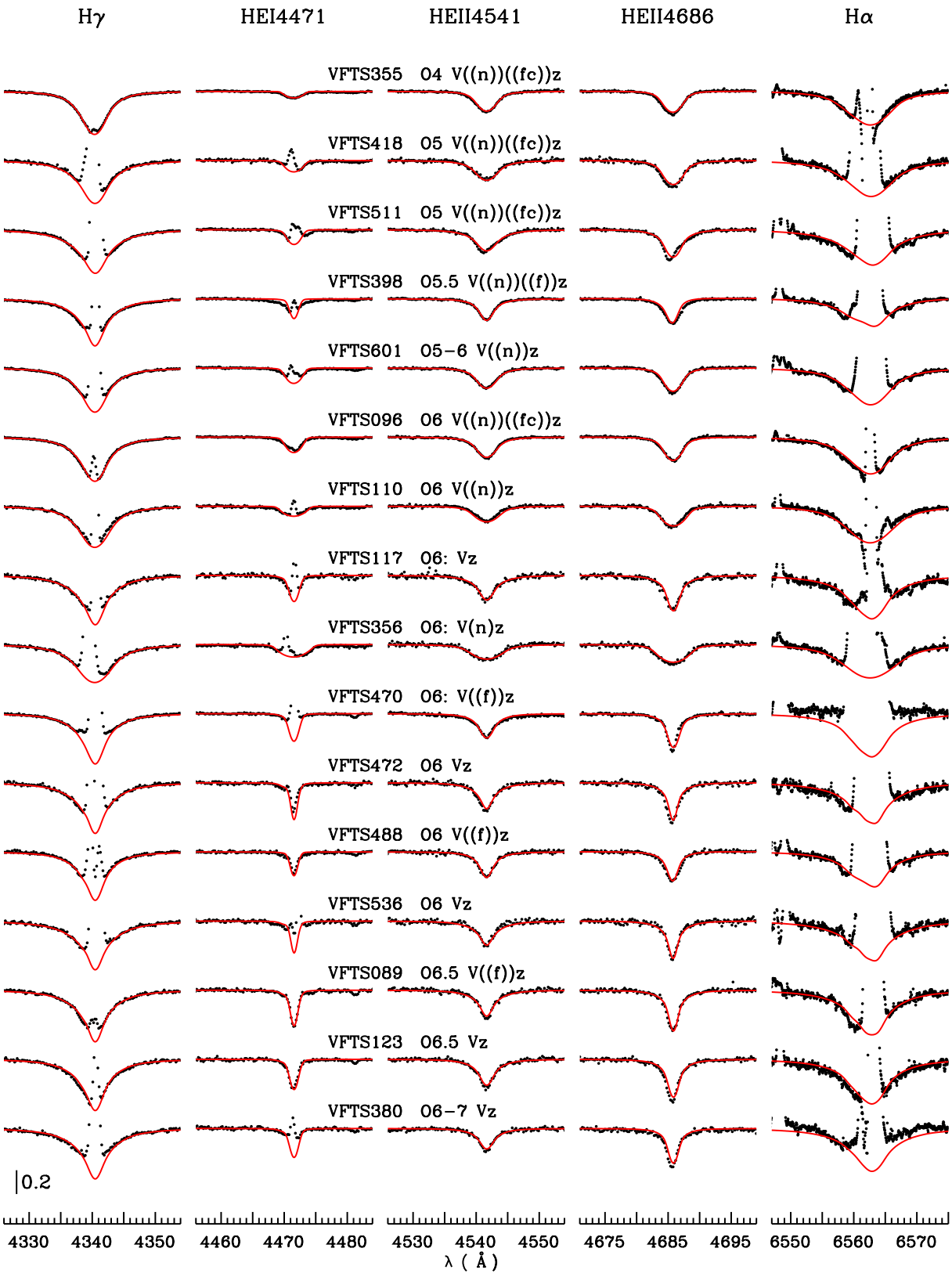

Fig. B.1. Observed spectra (black dots) and best-fitting synthetic models (red lines) of Hγ, He I λ4471, He II λ4541, He II λ4686 and Hα for the O Vz subsample. Each spectrum is labeled with its VFTS number and spectral classification. The cores of strong nebular lines have been removed.

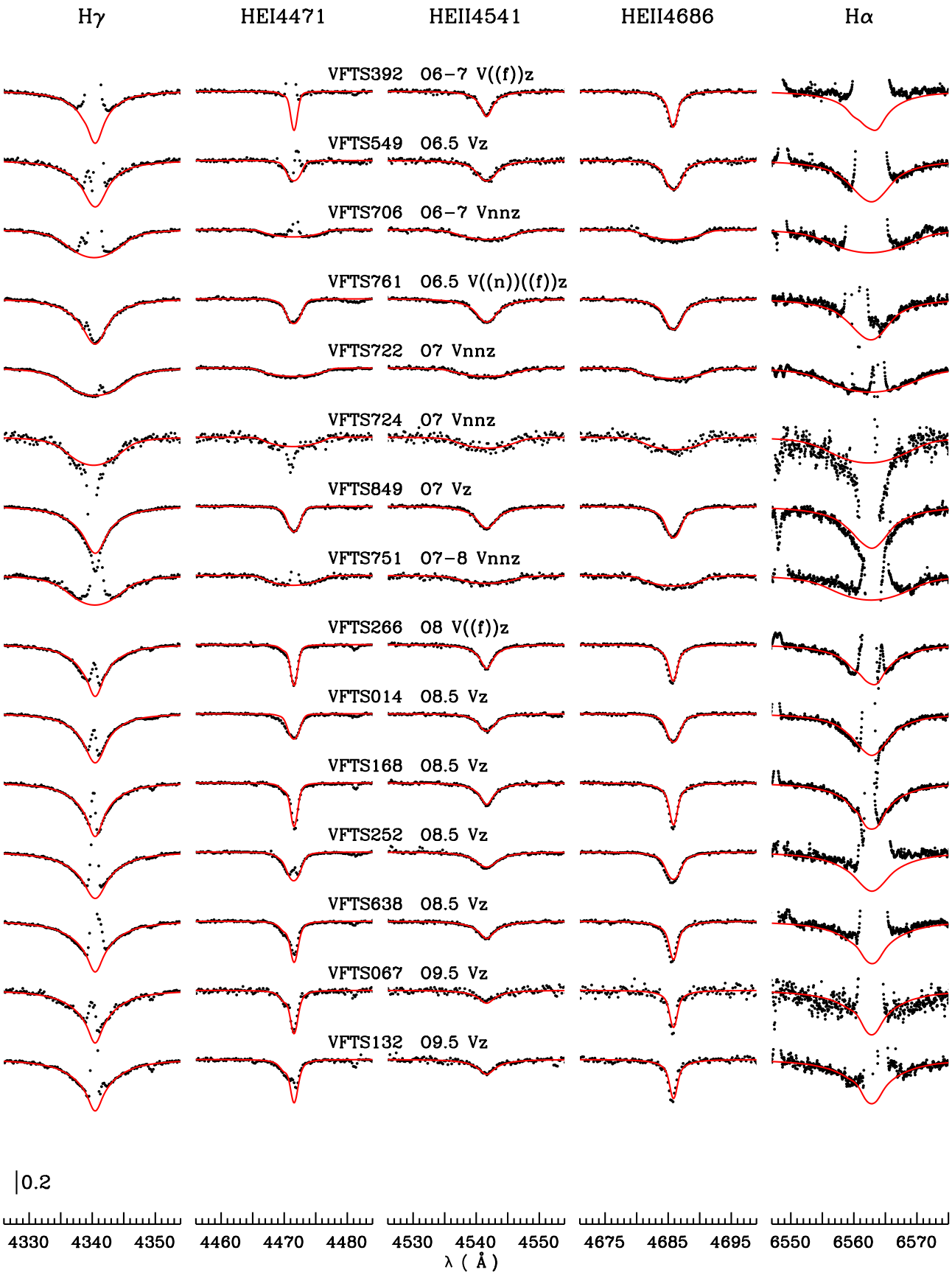

Fig. B.1. continued.

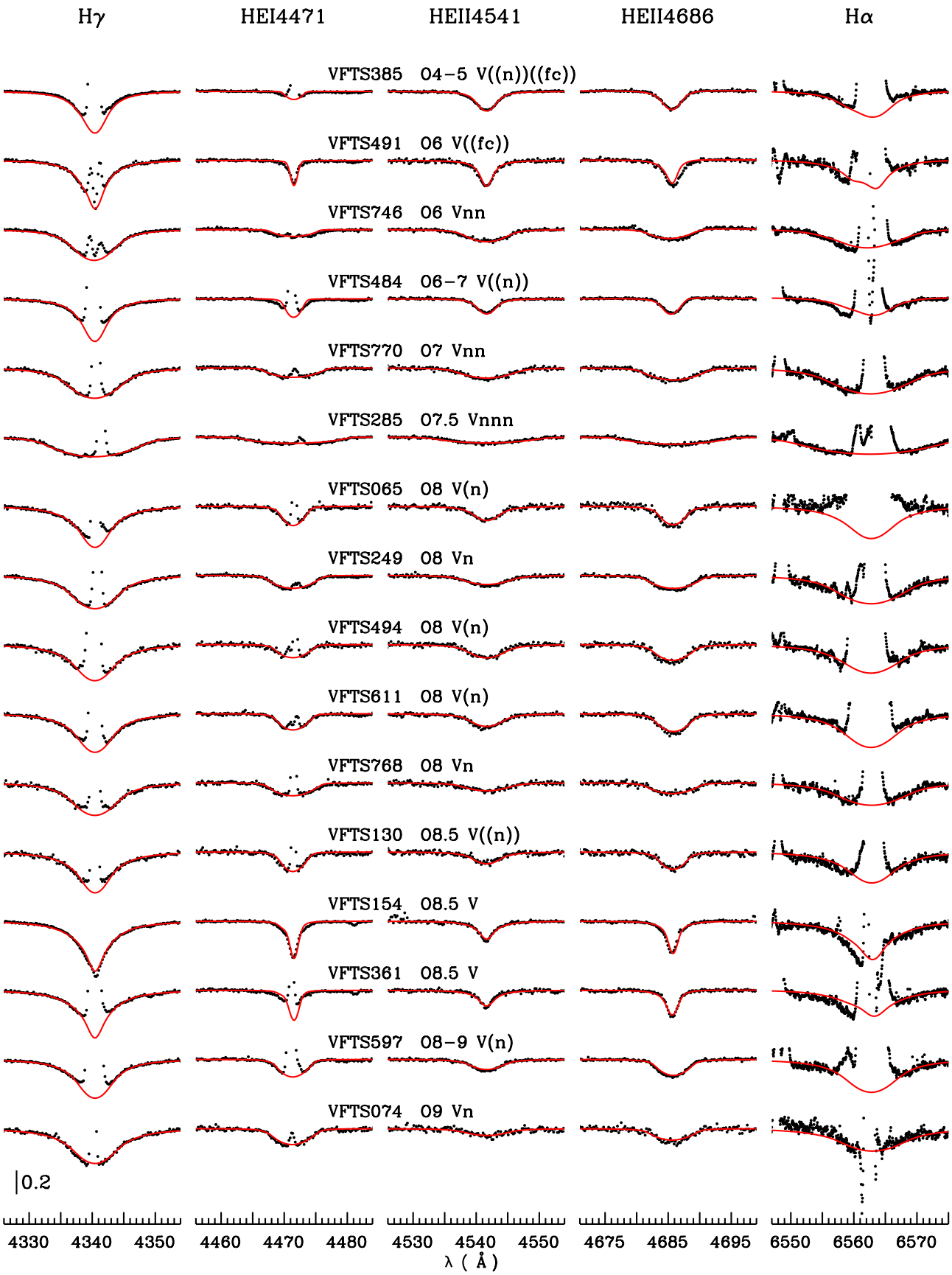

Fig. B.2. Observed spectra (black dots) and best-fitting synthetic models (red lines) for the O V subsample.

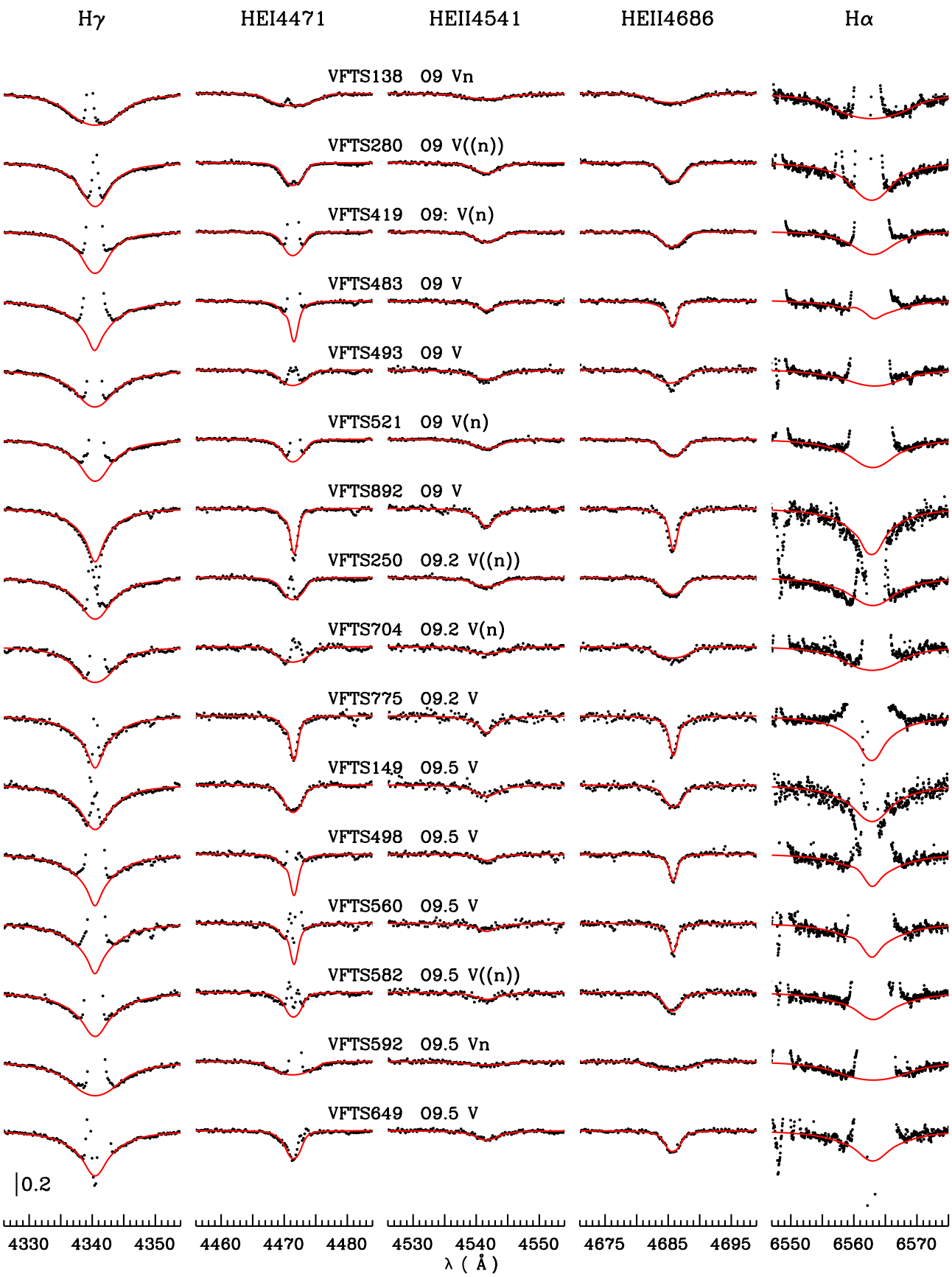

Fig. B.2. continued.

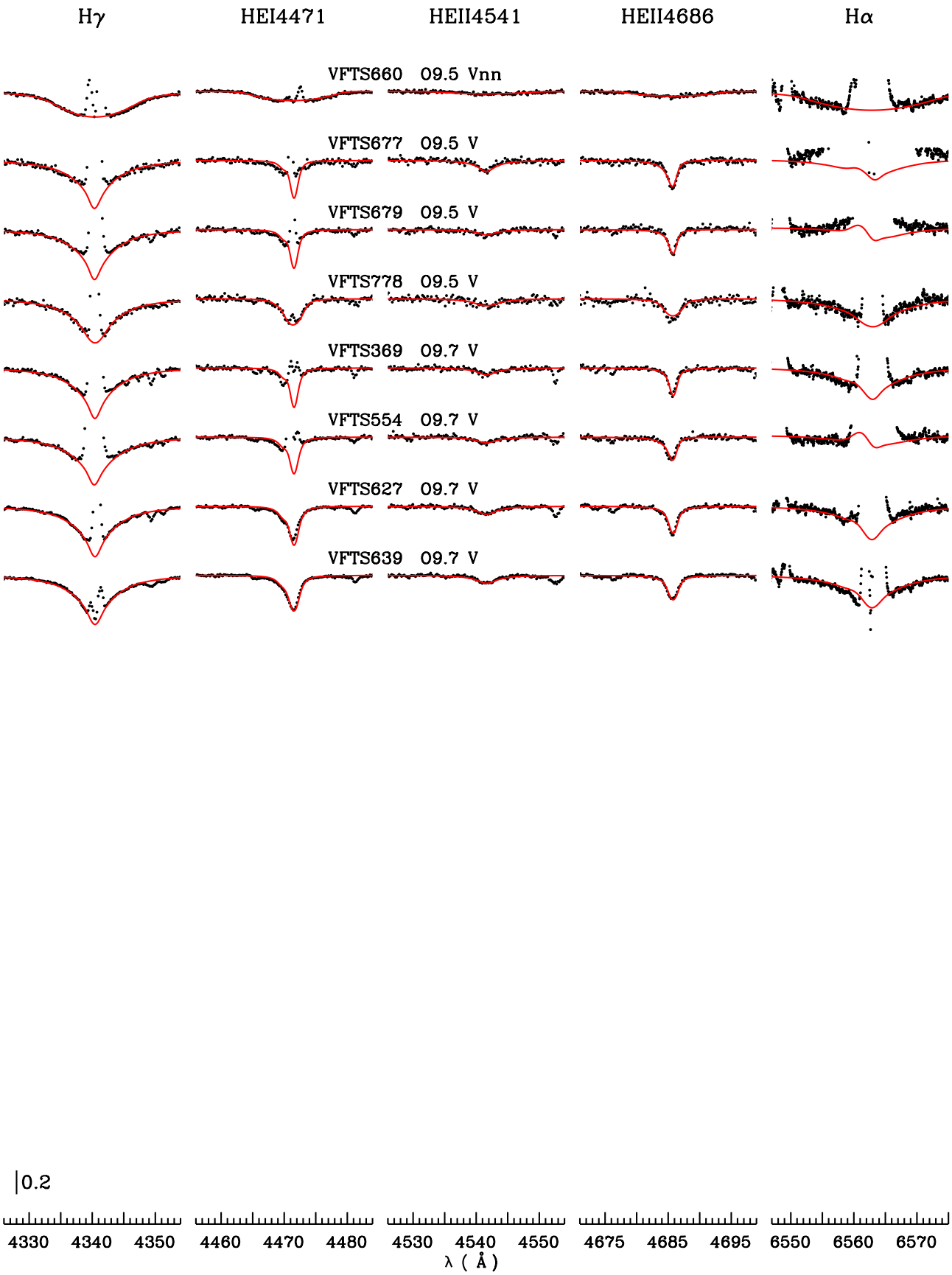

Fig. B.2. continued.

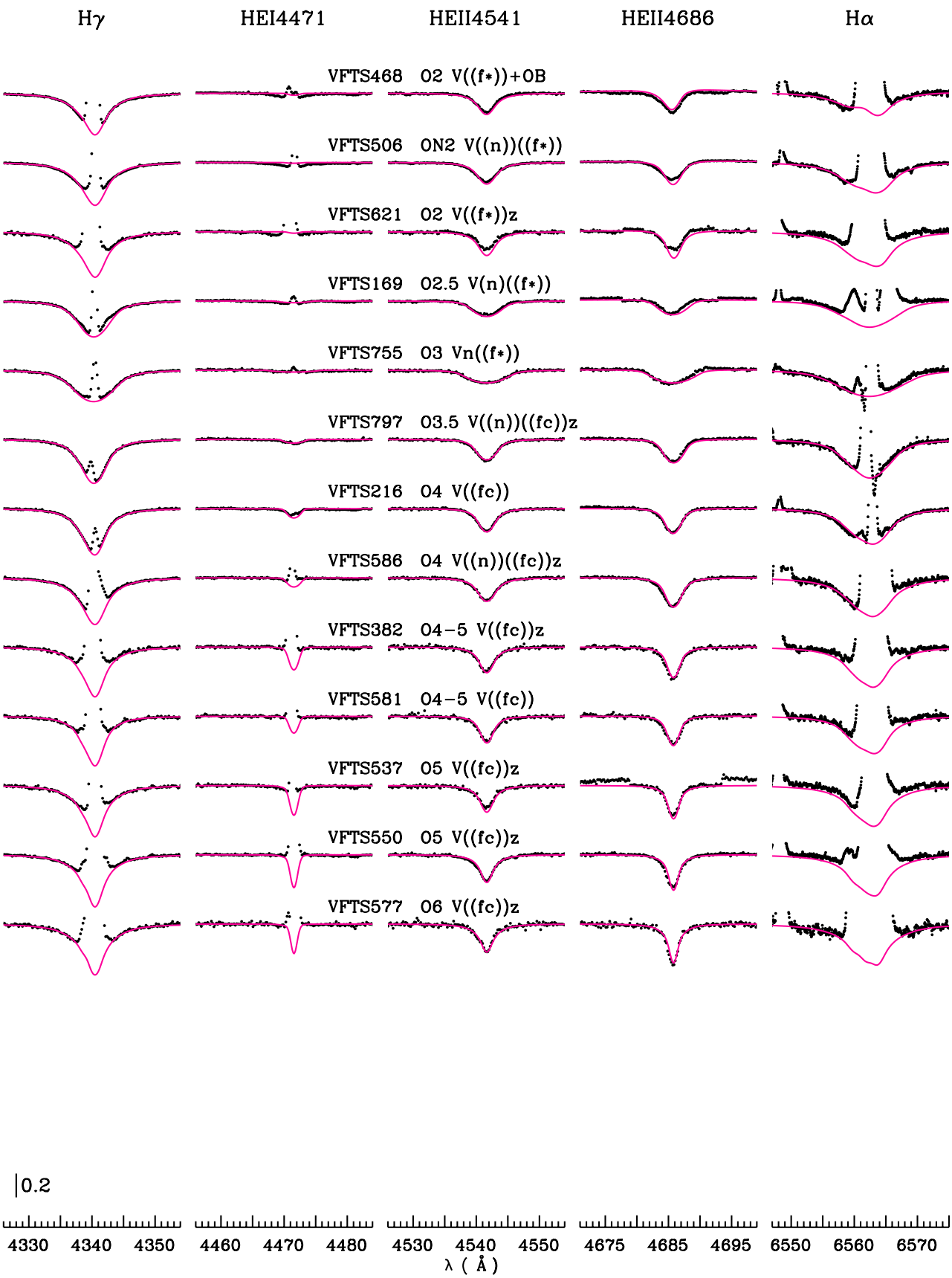

Fig. B.3. Observed spectra (black dots) and best-fitting synthetic models (pink lines) for the O Vz and O V stars analyzed using H, He and N as the diagnostic lines.